

1 **PROTEOMICS OF HYPOTHERMIC ADAPTATION REVEALS THAT RBM3**  
2 **ENHANCES MITOCHONDRIAL METABOLISM AND MUSCLE STEM-CELL**  
3 **DIFFERENTIATION**

4

5 Paulami Dey <sup>1,2</sup>, Srujanika Rajalaxmi <sup>1</sup>, Purvi Singh Thakur <sup>1</sup>, Maroof Athar Hashmi <sup>1,3</sup>, Heera  
6 Lal <sup>1,3</sup>, Nistha Saini<sup>1</sup>, Sneha Muralidharan <sup>1</sup>, Raviswamy G H Math <sup>1,4</sup>, Pushpita Saha <sup>1</sup>, Swarang  
7 Sachin Pundlik <sup>1,3</sup>, Nirpendra Singh <sup>1</sup>, Arvind Ramanathan <sup>1†</sup>

8

- 9 1. Institute for Stem Cell Science and Regenerative Medicine (inStem) GKVK - Post,  
10 Bellary Rd, Bengaluru, Karnataka 560065  
11 2. SASTRA deemed university, Tirumalaisamudram Thanjavur, Tamilnadu- 613401  
12 3. Manipal Academy of Higher Education, Manipal, Karnataka- 576104  
13 4. National Centre for Biological Sciences GKVK - Post, Bellary Rd, Bengaluru, Karnataka  
14 560065

15

16 **Abstract**

17 **Adaptation to hypothermic stress is important for skeletal muscle cells, but a**  
18 **comprehensive knowledge of molecular mediators is lacking. We show that adaptation to**  
19 **mild hypothermia (32<sup>o</sup>C) improves the ability of skeletal muscle myoblasts to differentiate**  
20 **into myotubes *in vitro*. We performed proteomic analysis of mouse myoblasts exposed to**  
21 **mild hypothermia for various time points and identified dynamic changes in**  
22 **mitochondrial metabolism and proteostasis. This revealed that RBM3, an RNA-binding**  
23 **protein, increases progressively with acute and chronic exposure to hypothermic stress,**  
24 **and is necessary for the enhanced differentiation upon hypothermic adaptation. We also**  
25 **demonstrate that overexpression of RBM3 at physiological temperatures is sufficient to (i)**  
26 **enhance mitochondrial metabolism as judged by a decrease in the AMPK energy-sensing**  
27 **pathway, (ii) increase levels of proteins associated with translation and increase levels of**  
28 **4E-BP1 phosphorylation, (iii) increase stem cell markers (MyoD1, PAX7), and improve**  
29 **differentiation of myoblasts from both young and aged mice.**

30

## 31 **Introduction**

32 Hypothermic adaptation is a hallmark of hibernating animals, and mild hypothermia has been  
33 used for preserving tissue homeostasis in patients, including the brain and heart<sup>1-6</sup>. During  
34 hypothermia, mitochondrial signaling maintains cellular energy homeostasis and promotes  
35 cellular survival<sup>7</sup>. It has been demonstrated that exposing human myoblasts to mild hypothermic  
36 conditions can improve their transplantation efficiency and survival. This observation can be  
37 leveraged for applications of myoblasts in cell-replacement therapies<sup>8</sup> and underlines the  
38 importance of uncovering comprehensive mechanisms that mediate hypothermic adaption.

39 In hibernating animals under hypothermic conditions (which can be as low as 0-5°C), one of the  
40 key RNA-binding proteins to be upregulated is RBM3 (RNA-binding motif protein 3) which is a  
41 cold-responsive protein<sup>9-13</sup>. RNA binding proteins (RBP) are characterized by the presence of an  
42 RNA binding domain (RBD) and an intrinsically disordered domain (IDD)<sup>14</sup>. RBPs are known to  
43 control gene expression through the regulation of protein synthesis and post-transcriptional  
44 processes like RNA splicing, RNA stability and RNA localization<sup>15,16</sup>. They are also known to  
45 affect cellular physiology in the context of numerous diseases e.g. neurodegenerative,  
46 cardiovascular disorders, cancer and hyperglycemia<sup>17-20</sup>.

47 RBM3 is a highly conserved glycine-rich protein with a molecular mass of 17 kDa which is  
48 known to be involved in neuroprotection and prevention of apoptosis<sup>21,22</sup>. In the context of  
49 skeletal muscles, RBM3 can inhibit atrophy in myotubes. Overexpression of RBM3 has been  
50 shown to promote survival against peroxide stress in myoblasts<sup>23,24</sup>. A recent study using C2C12  
51 cells has shown that RBM3 may bind to the 3' UTR and coding regions of mRNA involved in  
52 various cellular processes like translational initiation and proteasomal degradation<sup>25</sup>.

53 A comprehensive knowledge of proteomic changes during hypothermia in skeletal muscle cells  
54 is lacking. Therefore, mapping the hypothermic proteome and understanding the functional role  
55 of RBM3 in cells will enable new strategies for the application of therapeutic hypothermia. To  
56 fill this gap in understanding we performed a systematic temporal analysis of hypothermic  
57 adaptation using untargeted proteomics. Our study reveals that in response to both acute and  
58 chronic hypothermia myoblasts mount a dynamic response involving mitochondrial metabolism,

59 RNA processing and an increase in levels of RBM3. We show that overexpression of RBM3 in  
60 myoblasts at 37°C can recapitulate a subset of hypothermic effects on myoblast metabolism and  
61 differentiation in part by enhancing mitochondrial metabolism. Finally, we show that  
62 hypothermia and RBM3 can rejuvenate aged skeletal muscle precursor cells *in vitro* as judged by  
63 increased levels of stem cell markers (*Pax7*, *MyoD1*).

## 64 **Results**

### 65 **Hypothermic adaptation enhances the differentiation of mouse skeletal myoblasts**

66 To test the effects of hypothermic adaptation on skeletal muscle differentiation, we grew C2C12  
67 myoblasts at 32°C and 25°C respectively for 72 hrs. (37°C was used as control). This was  
68 followed by differentiation into myotubes at 37°C for 6 days (Fig 1A). We observed that the  
69 mRNA levels of differentiation markers like myosin heavy chain (*MyHC*, a late differentiation  
70 marker) and myogenin (*Myog*, an early differentiation marker) increased significantly under  
71 hypothermia as compared to the control (Fig 1 B, C, D, E). The protein levels of these markers  
72 also increased significantly during hypothermia, compared to the control (Fig 1 F, 1 G). We also  
73 observed that the increase in differentiation under hypothermia was more pronounced at 25°C  
74 compared to that at 32°C (Fig S1 A). We did similar experiments using mouse primary  
75 myoblasts isolated from wild-type B6/J mice. Primary myoblasts were grown at 32°C for 72 hrs.  
76 and then differentiated at 37°C for 6 days (37°C was used as a control). There was a loss of  
77 viability of primary myoblasts at 25°C unlike C2C12 cells (data not shown). Similarly to C2C12  
78 cells, we observed that both mRNA and protein levels of the differentiation markers significantly  
79 increased under hypothermia as compared to 37°C control (Fig 1 H, I, J). These results together  
80 imply that hypothermic adaptation in mouse skeletal myoblasts enhances differentiation.

### 81 **C2C12 cells grown under hypothermia (32°C) for 6, 12, 24 and 48 hrs. show a dynamic** 82 **increase in levels of proteins involved in RNA processing and cellular metabolism**

83 To understand underlying global changes under hypothermia, we performed proteomic profiling  
84 of C2C12 cells grown under hypothermia (32°C) at different time points. We grew C2C12 cells  
85 at 32°C for 6 hrs., 12 hrs., 24 hrs., and 48 hrs. and performed proteomic profiling using a  
86 SWATH proteomics workflow. We observed that among the 1347 proteins detected, 323  
87 proteins were upregulated at 6 hrs. (24%), 237 proteins were upregulated at 12 hrs. (17.6%), 284

88 proteins were upregulated at 24 hrs. (21%) and 300 proteins were upregulated at 48 hrs. (22%)  
89 respectively. 469 proteins were downregulated at 6 hrs. (34.9%), 393 proteins were  
90 downregulated at 12 hrs. (29.2%), 413 proteins were downregulated at 24 hrs. (30.7%) and 390  
91 proteins (29%) were downregulated at 48 hrs. respectively (Fig 3S A).

92 Hypothermia induced acute changes in protein levels at 6 hrs. and differential responses over 12  
93 hrs., 24 hrs., and 48 hrs. respectively (Fig 2 A, B, C). We observed that broadly hypothermia  
94 increased proteins involved in RNA processing, lipid metabolism, tricarboxylic acid (TCA), and  
95 electron transport chain (ETC) pathways. GO pathway and process enrichment analysis also  
96 indicated that pathways involved in carbon (monocarboxylic, amino acid, and energy)  
97 metabolism and RNA processing were progressively upregulated under hypothermia (Fig 3 A, B,  
98 C, D).

99 With respect to RNA metabolism and processing, at 6 hrs. there was a significant upregulation of  
100 proteins involved in translation initiation (eIF-3h, eIF-1, eIF-3i, eIF-3d, eIF-4G1, RPS27). At 48  
101 hrs. most of these proteins were not detectable but instead, proteins involved in RNA-splicing  
102 (PUF60, DDX15, USP39, SNRPB2), and RNA processing (DHX15, LSM8) were significantly  
103 upregulated. 12 hrs. and 24 hrs. showed upregulation of proteins present within both these sets.  
104 With respect to proteins associated with lipid metabolism, a set of unique proteins involved in  
105 beta-oxidation was upregulated at 6 hrs. (Fig S2 A). A subset of these proteins involved in beta-  
106 oxidation of fatty acids (ACAT1, ACADM, HADHA, ACAA1A, HSD17B4, HSD17B10), were  
107 detected at 24 hrs. and 48 hrs. respectively. With respect to the TCA pathway, three proteins,  
108 which are components of the mitochondrial pyruvate dehydrogenase complex (DLD, PDHB,  
109 PDHA1) were upregulated at 6 hrs., 12 hrs., 24 hrs., and 48 hrs. respectively. Succinate-CoA  
110 ligase (SUCLA2, SUCLG1) was not present at 6 hrs. and 12 hrs. but upregulated significantly at  
111 24 hrs. and 48 hrs.

112 Another set of unique proteins was upregulated only at 6 hrs., 12 hrs., 24 hrs., and 48 hrs.  
113 respectively and these included proteins involved in RNA splicing, RNA processing, lipid  
114 metabolism, TCA, ETC (Listed in Fig S2 A, B).

115 Cellular processes like RNA processing and metabolism, monocarboxylic acid metabolism,  
116 amino acid metabolism, acyl-CoA metabolism and splicing of RNA were upregulated under

117 hypothermia at different time points as shown by the Metascape analysis software<sup>26</sup>  
118 (summarized in Table 1, Fig S3 B, C, D, E).

119

### 120 **RBM3 is upregulated by hypothermic stress in C2C12 and mouse primary myoblasts**

121 RNA binding proteins (RBM) are a class of proteins that bind to double or single-stranded RNA.  
122 They contain an RNA-recognition motif (RRM) and are critical for RNA processing and stress  
123 response<sup>27</sup>. Two proteins belonging to the RBM family were upregulated in response to  
124 hypothermia: RBM3 and CIRBP (Cold inducible RNA binding protein). RBM3 was upregulated  
125 even at 6 hrs. and increased progressively till 48 hrs. whereas, CIRBP was expressed only at 24  
126 hrs. and its level decreased by 48 hrs. (Fig 2 D, E). Therefore, we investigated the role of RBM3  
127 in the hypothermic adaptation of myoblasts.

128 The mRNA levels of *RBM3* increased after 48 hrs. and 72 hrs. of hypothermia in C2C12 and  
129 mouse primary myoblasts (Fig 2 F, G).

130 By western blotting, we confirmed that protein levels of RBM3 increased after 48 hrs. and 72  
131 hrs. of hypothermia in C2C12 cells and mouse primary myoblasts (Fig 2 H, I).

132

### 133 **RBM3 is required for hypothermia-mediated enhanced C2C12 myoblast differentiation**

134 Since hypothermia was observed to promote differentiation of skeletal muscle myoblasts and  
135 RBM3 was upregulated during hypothermia, we hypothesized that hypothermia-dependent  
136 promotion of differentiation could be dependent on the expression of RBM3. To test this, C2C12  
137 cells were transfected with siRBM3 (scrambled siRNA was used as control) (Fig S4 A). After 48  
138 hrs. of siRNA treatment, we incubated the C2C12 myoblasts (siRBM3 transfected and scrambled  
139 siRNA transfected) at 32<sup>0</sup>C for 72 hrs. (37<sup>0</sup>C scrambled siRNA treated cells were used as  
140 control) followed by differentiation into myotubes at 37<sup>0</sup>C for 6 days. We observed that the  
141 mRNA levels of differentiation markers: *MyHC* and *Myog*, increased significantly at 32<sup>0</sup>C in  
142 scrambled siRNA-treated cells compared to 37<sup>0</sup>C scrambled siRNA-treated cells as expected.  
143 Conversely, we observed that cells treated with siRBM3 showed a decrease in differentiation  
144 markers after incubation at 32<sup>0</sup>C (Fig 4 A, B).

145

146 **Overexpression of RBM3 is sufficient to enhance differentiation of C2C12 and mouse**  
147 **primary myoblast at 37<sup>0</sup>C**

148 Since RBM3 was required for hypothermia-driven enhanced differentiation of myoblasts, we  
149 tested whether RBM3 was sufficient for enhanced differentiation of myoblasts at 37<sup>0</sup>C. We  
150 generated stable C2C12 cell lines overexpressing pMIG-RBM3 (pMIG-GFP was used as  
151 control) (Fig S4 B, C). Stable C2C12 cells (overexpressing RBM3) were grown at 37<sup>0</sup>C and  
152 differentiated at 37<sup>0</sup>C for 6 days. We observed that mRNA and protein levels of the  
153 differentiation marker MyHC increased significantly in C2C12 cells overexpressing RBM3  
154 compared to the control. This indicates that RBM3 can promote the differentiation of myoblasts  
155 in a hypothermia-independent manner (Fig 4 C, D).

156 We performed a similar experiment in mouse primary myoblasts where we transfected the  
157 primary cells with pMIG-RBM3 (pMIG-GFP was used as control) and differentiated them at  
158 37<sup>0</sup>C for 6 days. We observed similar results of increased mRNA levels of differentiation  
159 markers (*MyHC and Myog*) due to overexpression of RBM3. (Fig 4 F, G)

160

161 **Overexpression of RBM3 promotes C2C12 myoblasts viability and proliferation**

162 Next, we tested the effects of RBM3 on cell proliferation and cell viability of mouse skeletal  
163 myoblasts. We grew the stable lines of C2C12 cells on coverslips and stained them with Ki-67  
164 antibody and performed confocal microscopy to determine the mean integrated intensity of the  
165 Ki-67 positive nuclei. We observed that overexpression of RBM3 leads to an increase in the Ki-  
166 67 intensity. (Fig 4 H, I). We also performed a cell counting assay where we plated an equal  
167 number of cells (of both GFP and RBM3) respectively and counted the cell number from day 1  
168 to day 3. We observed that overexpression of RBM3 leads to an increase in cell proliferation in  
169 all three days (Fig 4 K). Next, we tested whether the overexpression of RBM3 affected cell  
170 viability. We grew the C2C12 cells in 96 well plates for two days and performed an MTT assay.  
171 We observed that overexpression of RBM3 increased cell viability compared to the control (Fig  
172 4 J). We also checked for the levels of the myoblast marker *MyoDI* in mouse primary cells  
173 transfected with RBM3 (GFP-transfected cells were used as control). We observed that mRNA

174 expression levels of *MyoD1* increased with overexpression of RBM3 compared to control cells  
175 (Fig S4 D). These observations suggest that overexpression of RBM3 promoted cell viability,  
176 proliferation of C2C12 myoblasts and increased expression levels of the undifferentiated  
177 myoblast marker.

178 **Overexpression of RBM3 in C2C12 myoblasts upregulates subsets of processes involved in**  
179 **hypothermia, specifically those involved in RNA processing, lipid, and mitochondrial**  
180 **metabolism**

181 Using proteomics, we observed that the overexpression of RBM3 significantly upregulated levels  
182 of proteins involved in RNA metabolism and processing: for example, proteins involved in  
183 proteasomal degradation (PSMC4, PSME2, PSMD14, PSMD6, PSMD8) and RNA splicing  
184 (SNRNP200, SF3B5, SRRM2). We found proteins involved in lipid metabolism (ACADL,  
185 ACADSB, ME2, ECHS1, FABP5) to be upregulated. Proteins involved in ETC (NDUFA5,  
186 NDUFA2, NDUFV1) were also upregulated (Fig 5 A, B, C). Cellular processes like RNA  
187 metabolism, fatty acid metabolism, ribonucleoprotein complex biogenesis, and RNA localization  
188 were upregulated significantly as analyzed by Metascape software (Fig 5 E). GO pathway and  
189 process enrichment analysis revealed that pathways involved in the RNA metabolism, RNA  
190 localization, and fatty acid metabolism were upregulated due to overexpression of RBM3 (Fig S5  
191 A). We compared the hypothermia-responsive proteome and the RBM3 overexpression-  
192 responsive proteome. Of the 300 proteins that were upregulated during chronic exposure to  
193 hypothermia (48 hrs.) and 302 upregulated proteins during overexpression of RBM3, seventy-  
194 seven proteins were upregulated under both these conditions. Of this subset, several proteins  
195 were involved in lipid and mitochondrial pathways (Fig 5 D). Based on these observations we  
196 performed a lipidomic analysis of C2C12 overexpressing pMIG-RBM3 (pMIG-GFP was used as  
197 control). We observed that overexpression of RBM3 decreased the levels of triglycerides (TG)  
198 and cholesterol esters compared to the control (S9 A, B). This revealed a systemic rewiring of  
199 the metabolism of myoblasts by RBM3.

200

201 **Overexpression of RBM3 promotes mitochondrial metabolism, levels of intracellular**  
202 **Acetyl-CoA, and levels of the PKM2 splice variant**

203 Since our proteomic studies revealed that overexpression of RBM3 increased the lipid and  
204 mitochondrial metabolic processes, we next investigated levels of associated metabolic  
205 pathways.

206 We performed a seahorse analysis of stable C2C12 cells- overexpressing RBM3 (pMIG-RBM3)  
207 (pMIG-GFP was used as control) to measure oxygen consumption rate (OCR) of the cells, under  
208 basal conditions and in the presence of metabolic inhibitors (Fig 6 A). Overexpression of RBM3  
209 increased the basal respiration of C2C12 myoblasts compared to the control. The maximum  
210 respiration, spare respiratory capacity, and ATP-linked respiration increased in cells  
211 overexpressing RBM3 compared to the control (Fig 6 B). This suggests that RBM3 mediates an  
212 improvement in the oxygen consumption rate.

213 We performed an MTT assay to test the viability of cells overexpressing RBM3 in the presence  
214 of mitochondrial and glycolytic inhibitors. We observed a decreased sensitivity of cells  
215 overexpressing RBM3 to oligomycin (mitochondrial complex V inhibitor) and 2DG (2-  
216 deoxyglucose, a competitive inhibitor of glucose) compared to the control (Fig S6 A, C), as  
217 judged by the increase in the IC50 value of the inhibitors in cells overexpressing RBM3  
218 compared to the control (Fig S6 B, D).

219 Since we observed an increase in mitochondrial oxygen consumption rate in cells overexpressing  
220 RBM3, we tested if there is any difference in mitochondrial morphology or mitochondrial  
221 membrane potential using mitotracker and TMRM staining respectively. We observed no  
222 significant differences in mitochondrial morphology and membrane potential due to the  
223 overexpression of RBM3 (Fig S7 A, B).

224 We measured both intracellular and extracellular levels of glycolytic and TCA intermediates. We  
225 observed that intracellular levels of pyruvate, lactate, malate, succinate, glutamate, and fumarate  
226 increase in cells overexpressing RBM3 compared to the control. Whereas extracellular levels of  
227 lactate, glutamate, and fumarate decrease in cells overexpressing RBM3, and levels of malate,  
228 succinate and pyruvate, citrate, and isocitrate increase due to overexpression of RBM3 (Fig 6 C,  
229 D). Intracellular lactate/pyruvate ratio decreased in cells overexpressing RBM3 compared to the  
230 control (Fig S7 F, G). Intracellular acetyl-CoA levels were significantly increased in cells  
231 overexpressing RBM3 compared to the control (Fig 6 E). Concomitantly we observed that  
232 overexpression of RBM3 was associated with an increase in protein levels of pyruvate

233 dehydrogenase (PDH) (Fig S7 C, D) and pyruvate kinase isoform 2 (PKM2) (Fig 6 F, G, H)  
234 whereas there was a decrease in succinate dehydrogenase (SDHA, SDHC) (Fig S7 C, D) and  
235 pyruvate kinase isoform1 (PKM1) (Fig 6 F, G, H). We measured the expression levels of mRNA  
236 of *Pkm1*, *Pkm2*, *Sdha*, *Sdhc*, *Pdhb* in mouse primary myoblasts and observed a decrease in *Pkm1*,  
237 *Sdha*, *Sdhb*, *Pdhb* and an increase in *Pkm2* (Fig 6I, S7 E).

238

239 **Overexpression of RBM3 (i) decreases phosphorylation of AMPK-beta (Ser 182), (ii)**  
240 **decreases phosphorylation of acetyl-CoA carboxylase (ACC) (Ser 79) and (iii) increases**  
241 **phosphorylation of 4E-BP1 (Thr 37/46)**

242

243 RBM3 increased mitochondrial metabolism (Fig 6) and one of the key sensors of mitochondrial  
244 bioenergetics is AMP-activated protein kinase (AMPK)<sup>27-29</sup>. Therefore, we analysed the levels of  
245 phosphorylation of AMPK subunits and its direct phosphorylation target (ACC)<sup>30,31</sup>. Western-  
246 blot analysis of C2C12 cells overexpressing RBM3 (using GFP as control) showed a decrease in  
247 the levels of phosphorylation of AMPK-beta (Ser 182) (Fig 6J, K, L). We observed a decrease in  
248 levels of phosphorylation of ACC (Ser 79) (Fig 6J, K, L). We did not observe any significant  
249 change in the ratio of phosphorylated to total AMPK-alpha (Fig S7 H, I, J).

250 Overexpression of RBM3 increased the levels of proteins involved in translation initiation (Fig 5  
251 A) and phosphorylation of 4E-BP1 is known to promote cap-dependent translation.  
252 Phosphorylation of 4E-BP1 (Thr 37/46) is mediated by mTOR and it primes 4E-BP1 for getting  
253 phosphorylated at Ser 65/70 which can subsequently lead to activation of cap-dependent  
254 translation<sup>32</sup>. Therefore, we measured the levels of phosphorylated 4E-BP1. We observed an  
255 increase in the levels of phosphorylation of 4E-BP1 (Thr 37/46) with overexpression of RBM3  
256 (Fig 6 J, K, L).

257

258 **Myoblasts from aged mice have a diminished ability to differentiate *in vitro* which is**  
259 **partially rescued by hypothermia**

260 We evaluated whether hypothermic adaptation could improve the differentiation of aged mouse  
261 myoblasts. We isolated mouse myoblasts from aged (18 months old) and young (2-3 months old)  
262 wild-type mice (B6/J) and cultured them at 37<sup>0</sup>C followed by differentiation at 37<sup>0</sup>C for 5 days.  
263 A decrease in *MyHC* and *Myog* mRNA levels was observed in the case of aged cells as  
264 compared to the young ones (Fig S10 A, B). Additionally, we observed a decrease in the mRNA  
265 levels of stem cell marker (*Pax7*) and myoblast markers like *Myf5* and *MyoD1* in aged cells  
266 compared to young cells (Fig 7A, B, C). We next cultured the aged myoblasts in hypothermia  
267 (32<sup>0</sup>C for 72 hrs.) followed by differentiation at 37<sup>0</sup>C for 5 days (37<sup>0</sup>C was used as control). We  
268 observed that hypothermia increased the levels of *MyHC* (Fig 7 D) and *Myog* (Fig S10 C) in  
269 aged cells compared to the control. Also, the mRNA levels of *RBM3* increased as expected after  
270 hypothermia in aged myoblasts (Fig 7 E).

271

## 272 **Overexpression of RBM3 increases mRNA and protein expression of myoblast markers in** 273 **aged cells**

274 Next, we tested whether overexpression of RBM3 was sufficient to increase the expression of  
275 stemness markers and enhance the differentiation of aged myoblasts. We transfected aged  
276 myoblasts with pMIG-RBM3 (pMIG-GFP was used as control). We observed that  
277 overexpression of RBM3 in aged cells increased the mRNA expression levels of the stem cell  
278 marker, *Pax7* and myoblast markers, *MyoD1* and *Myf5* and proteins levels of MyoD1 compared  
279 to the control (Fig 7G, H, I). We measured extracellular levels of lactate, pyruvate and TCA  
280 cycle intermediates (Malate, Succinate, Fumarate). We observed that at 24 and 48 hrs., there was  
281 a time-dependent increase in extracellular levels of TCA cycle intermediates in RBM3  
282 overexpressing cells although these were not statistically significant (Fig S10 E, F).

283

## 284 **Discussion**

285 Therapeutic hypothermia is used for treatment in patients when there is a need for preserving  
286 tissue homeostasis in cases of brain or cardiac injury<sup>1,2,4,5</sup>. Hypothermia is also known to  
287 improve the transplantation efficiencies of human satellite cells<sup>21</sup>. Although this is a well-known  
288 phenomenon, the molecular players in the context of skeletal muscle remain poorly understood.

289 Uncovering these molecular players has key implications for new therapeutic targets in  
290 preserving or promoting skeletal muscle homeostasis. In agreement with previous observations,  
291 we found in our study that hypothermic adaptation in both C2C12 and primary myoblasts  
292 enhanced the ability of myoblasts to differentiate as judged by the mRNA- levels of  
293 differentiation markers. To understand the dynamics and dissect pathways and mechanisms  
294 underlying hypothermic adaptation we grew C2C12 cells at 32<sup>0</sup>C for multiple time points (6, 12,  
295 24, and 48 hrs.) and performed unbiased proteomic profiling of intracellular proteins. We  
296 discovered a proteome-wide rewiring in response to both acute (6 hrs.) and chronic (48 hrs.)  
297 hypothermia in C2C12 myoblasts. Interestingly we observed that out of 1347 detectable proteins,  
298 25% were upregulated as early as 6 hrs., and this reduced to approximately 21% at 48 hrs. (Fig  
299 S3 A). Concomitantly we observed a subset of translation initiation factors (eIF-3d, eIF-3i, eIF-  
300 1) and proteins associated with the proteasomal machinery (PSMD1, PSMD3, PSME4, PSMB4)  
301 to be upregulated as early as 6 hrs., indicating that these pathways play critical in rewiring the  
302 proteome during hypothermia (Fig 2 A, Fig S2 B). We also observe a subset of proteins involved  
303 in splicing and RNA metabolism to be upregulated during hypothermia suggesting that RNA  
304 metabolism and splicing play also play an important role. A significant part of the proteome was  
305 downregulated during hypothermia. 34.9% of proteins were downregulated at an early time-point  
306 of 6 hrs. which decreased to 29% at 48 hrs. (Fig S3 A). While a subset of translation factors  
307 increased during hypothermia, there was a subset of translation factors that were also  
308 downregulated during hypothermia (eIF-3A, eIF-3F, eIF-3B) (data not shown) suggesting a  
309 context-dependent role for these factors. Apart from RNA metabolism, some of the proteins  
310 involved in mitochondrial metabolism; TCA (SUCLA2, SUCLG1), ETC (NDUFS, COX,  
311 ATP5), and lipid metabolism (ACADM, ACADSB) increased in levels during hypothermia (Fig  
312 2 A, Fig S2 A).

313 Two RNA-binding proteins increased in levels during hypothermia: RBM3 (RNA binding motif  
314 protein 3) and CIRBP (Cold inducible RNA-Binding protein). RBMs (RNA binding proteins) are  
315 a class of proteins known to be involved in the regulation of RNA. RBM3 was seen to be  
316 upregulated from early time points of 6 hrs. and gradually increased till 48 hrs. but CIRBP was  
317 downregulated during early time points but upregulated at later time points of 24 hrs. and 48 hrs.  
318 (Fig 2 D, E). Few other RNA-binding proteins like RBM25, RBM39, and RO60 were  
319 significantly downregulated.

320 RBM3 is a 17 kDa protein that consists of an RNA-binding domain (RBD) and an (IDD)<sup>14</sup>. It has  
321 been previously shown that RBM3 is neuroprotective and promotes cellular proliferation in  
322 neurons<sup>22,23</sup>. It has also been previously shown that RBM3 can protect myoblasts against ROS  
323 stress<sup>24</sup>. A comprehensive measurement of molecular changes that mediate the effect of  
324 hypothermia and RBM3, especially in the context of skeletal muscle function have remained less  
325 understood. In this study, we have shown that hypothermia-mediated enhancement in skeletal  
326 muscle differentiation is dependent on RBM3 expression (Fig 4 A, B). Furthermore, we observed  
327 that overexpression of RBM3 is sufficient to promote skeletal muscle differentiation,  
328 independent of hypothermia (Fig 4 C, D, E) We also find that overexpression of RBM3 increases  
329 cell growth rate increases cell viability, and enhances the levels of stemness markers like and  
330 MyoD1 in skeletal muscle myoblasts (Fig 4 H, I, J, K, Fig S4 C). We performed a proteomics  
331 analysis of C2C12 cells overexpressing RBM3 to understand cellular processes that are under its  
332 control. We observed increased levels of proteins involved in processes associated with RNA  
333 metabolism, similar to that observed in hypothermia (Fig 2 A, 5 A). These included proteins  
334 involved in splicing (SF3B5, SRRM2), proteasomal degradation machinery (PSMD6, PSME4,  
335 PSMC4, PSMD8). We also observed that the ratio of PKM2 to PKM1 proteins is increased in  
336 RBM3 overexpressing cells. PKM1 and PKM2 are splice variants of the glycolytic enzyme  
337 pyruvate kinase, and increased PKM2 is a marker of a stem cell state<sup>33</sup>. The increased PKM2  
338 levels in RBM3 overexpression indicate an increased proliferation of cells overexpressing RBM3  
339 compared to the control (Fig 4H, K). These results indicate that RBM3 is involved in the  
340 regulation of splicing in myoblasts.

341 We also observed an increase in levels of ribosomal proteins (RPS27A, RPL5, RPS27) involved  
342 in translation from the proteomic analysis (Fig 5 A). It is known that 4E-BP1 activates cap-  
343 dependent translation. mTOR mediates phosphorylation of 4E-BP1 (Thr 37/46) and it allows 4E-  
344 BP1 to get phosphorylated at Ser 65/70 which can subsequently lead to activation of cap-  
345 dependent translation<sup>32</sup>. Therefore, we hypothesized that overexpression of RBM3 can affect the  
346 phosphorylation of 4E-BP1 (Thr 37/46) thereby affecting translation. In this study, we observed  
347 an increase in the levels of phosphorylation of 4E-BP1 (Thr 37/46) with overexpression of  
348 RBM3. This suggests an activation of cap-dependent translation in cells overexpressing RBM3  
349 (Fig 6J, K, L). Proteomic analysis of myoblasts overexpressing RBM3 suggests an increase in

350 the levels of proteins involved in mitochondrial metabolism including lipid metabolism  
351 (ACADL, ACASB) and ETC (NDUFS) (Fig 5 B, C).

352 Overall, this shows that RBM3 can recapitulate aspects of hypothermia even at room  
353 temperature.

354 As RBM3 upregulated levels of proteins involved in lipid metabolism, like beta-oxidation of  
355 fatty acids, we performed lipidomics analysis of RBM3 overexpressed cells, We found that the  
356 levels of triglycerides and cholesterol esters were decreased in cells overexpressing RBM3 (Fig  
357 S9).

358 This suggests that RBM3 may cause increased mobilization of fatty acids which correlates with  
359 decreased levels of triglycerides. The decrease in cholesterol esters may imply the role of RBM3  
360 in cholesterol metabolism as well. In this context, the increased intracellular levels of acetyl-CoA  
361 could be indicative of enhanced beta-oxidation of lipids (Fig 6 E).

362 In order to gain a deeper perspective of the role of RBM3 in regulating metabolism, we analyzed  
363 oxygen consumption using a Seahorse instrument. We showed that overexpression of RBM3  
364 improved basal respiration. The maximum respiration of the cells after treatment with the  
365 uncoupler FCCP also increased in the presence of RBM3 (Fig 6 A, B). This could suggest an  
366 increase in the levels of proteins involved in the electron transport chain. In agreement with this,  
367 from the proteomics analysis, we observed an increase in mitochondrial ETC proteins like the  
368 complex I proteins NDUF1, NDUF3 and NDUFV1 (Fig 5 C). The TMRM and mitotracker  
369 imaging experiment revealed no significant change in mitochondrial membrane potential and  
370 mitochondrial morphology (Fig S7 A, B). This suggests that an increase in maximal respiration  
371 could be due to an increase in the levels of proteins involved in the mitochondrial electron  
372 transport chain, and not the overall mitochondrial biogenesis. To further verify these results, we  
373 performed metabolomics analysis of intracellular and extracellular TCA and glycolytic  
374 metabolites. We observed that the intracellular levels of citrate, pyruvate, succinate, and malate  
375 increased overexpressing RBM3. Concomitantly extracellular levels of citrate and isocitrate were  
376 increased, supporting an enhanced mitochondrial metabolism upon overexpression of RBM3  
377 (Fig 6 C, D).

378 We observed an increase in mitochondrial oxygen consumption rate (OCR) and ATP-linked  
379 respiration in cells overexpressing RBM3 (Fig 6A, B) which shows increased mitochondrial  
380 metabolism. It is known that AMPK plays a vital role in regulating mitochondrial energy  
381 homeostasis by sensing the levels of intracellular AMP<sup>8</sup>. AMPK is a heterotrimeric enzyme  
382 complex containing alpha, beta and gamma subunits<sup>29-31</sup>. Under conditions of energy-stress  
383 (high AMP to ATP ratio) in the cell, AMPK undergoes phosphorylation including the beta  
384 subunit (Ser 182)<sup>34</sup>. Upon phosphorylation, AMPK phosphorylates its canonical substrate ACC  
385 (Ser 79) and enhances catabolic processes in cells<sup>29-31</sup>. We hypothesized that an increase in  
386 mitochondrial metabolism by RBM3 could decrease the phosphorylation of AMPK. In  
387 agreement with this, we observed that overexpression of RBM3 decreases the level of  
388 phosphorylation of AMPK-beta (Ser 182) and its canonical substrate ACC (ser 79). Overall, this  
389 suggests improved energy homeostasis in cells overexpressing RBM3 (Fig 6J, K, L).

390 It is known that mitochondrial oxidative phosphorylation and bioenergetics play an important  
391 role in the ageing of muscle stem cells<sup>35</sup>. AMPK is a key node regulating mitochondrial  
392 metabolism and has been implicated in ageing<sup>36-38</sup>. Since we have shown that RBM3 enhances  
393 mitochondrial metabolism and affects AMPK phosphorylation, therefore we tested the effect of  
394 RBM3 in the rejuvenation of aged satellite cells. It has been shown that satellite cells from aged  
395 muscles have diminished regenerative capacity both due to cell-autonomous and non-  
396 autonomous factors<sup>39</sup>. RBM3 is highly expressed in long-lived strains of mice and has been  
397 shown to increase the survival of C2C12 cells under ROS and ER stress<sup>24,40</sup>. We explored the  
398 causal role of RBM3 in diminishing markers of ageing in satellite cells isolated from aged mice.  
399 We show that overexpression of RBM3 can rejuvenate ageing skeletal muscle myoblasts as  
400 judged by the increased expression levels of the canonical satellite cell marker (*Pax7*) and  
401 myoblasts markers (*MyoD1* and *Myf5*) (Fig 7G, H, I, J). Moreover, we also show that  
402 overexpression of RBM3 increases the ability of aged myoblasts to produce higher levels of  
403 extra-cellular TCA intermediates e.g., succinate, malate and fumerate (Fig S10 G, H). Overall,  
404 this suggests that RBM3 may enhance satellite cell markers and metabolism *in vitro*. The study  
405 shows that RBM3 may intersect with pathways important for rejuvenating myoblasts from both  
406 young and old mice. It also provides an important underlying mechanism by which the  
407 hypothermic cells control multiple aspects of cellular physiology like RNA metabolism, splicing,  
408 mitochondrial metabolism and lipid metabolism. Our study shows that RBM3 in skeletal muscle

409 cells may define an important signaling hub that can be targeted both to improve metabolism and  
410 rejuvenate aged myoblasts.

411 Here we have shown that RBM3 directly controls the metabolism of muscle stem cells and their  
412 regenerative capacity *in vitro*. In the future, it will be important to determine the effect of RBM3  
413 overexpressing myoblasts during skeletal muscle regeneration *in vivo*. The direct targets of  
414 RBM3 (both mRNA and protein) that mediate its effects remain less understood. It is possible  
415 that RBM3 (like other RNA binding proteins containing the RRM and disordered domains) may  
416 form aggregates like stress granules and it might control the lifetime and translation of specific  
417 RNAs involved in metabolism. The molecular mechanisms governing the choice and regulation  
418 of RNA targets of RBM3 are yet to be understood<sup>41,42</sup>. Overall, controlling the expression of  
419 RBM3 using physiological conditions or small molecules presents an important avenue for  
420 regulating the stem cell state and metabolism.

421

422

## 423 **Main references**

- 424 1. Andresen, M., Gazmuri, J. T., Marín, A., Regueira, T. & Rovegno, M. Therapeutic  
425 hypothermia for acute brain injuries. *Scandinavian Journal of Trauma, Resuscitation and*  
426 *Emergency Medicine* vol. 23 (2015).
- 427 2. Gocoł, R. *et al.* The role of deep hypothermia in cardiac surgery. *International Journal of*  
428 *Environmental Research and Public Health* vol. 18 (2021).
- 429 3. Kochanek, P. M. Bakken Lecture: The brain, the heart, and therapeutic hypothermia.  
430 *Cleve. Clin. J. Med.* **76**, (2009).
- 431 4. Matsuzaki, M. *et al.* Impact of induced therapeutic hypothermia by intravenous infusion  
432 of ice-cold fluids after hospital arrival in comatose survivors of out-of-hospital cardiac  
433 arrest with initial shockable rhythm. *Circ. J.* **85**, 1842–1848 (2021).
- 434 5. Park, Y. *et al.* Therapeutic hypothermia reduces inflammation and oxidative stress in the  
435 liver after asphyxial cardiac arrest in rats. *Acute Crit. Care* **35**, 286–295 (2020).

- 436 6. Schäfer, A., Bauersachs, J. & Akin, M. Therapeutic Hypothermia Following Cardiac  
437 Arrest After the TTM2 trial – More Questions Raised Than Answered. *Curr. Probl.*  
438 *Cardiol.* **48**, 101046 (2023).
- 439 7. Lubawy, J., Chowański, S., Adamski, Z. & Słocińska, M. Mitochondria as a target and  
440 central hub of energy division during cold stress in insects. *Frontiers in Zoology* vol. 19  
441 (2022).
- 442 8. Drake, J. C. *et al.* Mitochondria-localized AMPK responds to local energetics and  
443 contributes to exercise and energetic stress-induced mitophagy.  
444 doi:10.1073/pnas.2025932118/-/DCSupplemental.
- 445 9. Fedorov, V. B. *et al.* Elevated expression of protein biosynthesis genes in liver and muscle  
446 of hibernating black bears (*Ursus americanus*). *Physiol. Genomics* **37**, 108–118 (2009).
- 447 10. Fedorov, V. B. *et al.* Modulation of gene expression in heart and liver of hibernating black  
448 bears (*Ursus americanus*). (2011).
- 449 11. Yan, J., Barnes, B. M., Kohl, F. & Marr, T. G. Modulation of gene expression in  
450 hibernating arctic ground squirrels. *Physiol Genomics* **32**, 170–181 (2008).
- 451 12. Williams, D. R. *et al.* Seasonally hibernating phenotype assessed through transcript  
452 screening Seasonally hibernating phenotype assessed through transcript screening.  
453 *Physiol Genomics* **24**, 13–22 (2005).
- 454 13. Yan, J., Barnes, B. M., Kohl, F. & Marr, T. G. Modulation of Gene Expression in  
455 Hibernating Arctic Ground. (2015) doi:10.1152/physiolgenomics.00075.2007.
- 456 14. Ciuzan, O., Hancock, J., Pamfil, D., Wilson, I. & Lodomery, M. The evolutionarily  
457 conserved multifunctional glycine-rich RNA-binding proteins play key roles in  
458 development. 1–11 (2015) doi:10.1111/ppl.12286.
- 459 15. Pelt, X. D. W. Van, Hettinger, Z. R. & Vanderklish, P. W. Translational Control of  
460 Muscle Mass RNA-binding proteins : The next step in translating skeletal muscle  
461 adaptations ? 654–660 (2023) doi:10.1152/jappphysiol.00076.2019.
- 462 16. Gerstberger, S., Hafner, M. & Tuschl, T. A census of human RNA-binding proteins. *Nat.*

- 463 *Rev. Genet.* **15**, 829–845 (2014).
- 464 17. Leon, B. M. Diabetes and cardiovascular disease: Epidemiology, biological mechanisms,  
465 treatment recommendations and future research. *World J. Diabetes* **6**, 1246 (2015).
- 466 18. Wang, J., Liu, Q. & Shyr, Y. Dysregulated transcription across diverse cancer types  
467 reveals the importance of RNA-binding protein in carcinogenesis. *BMC Genomics* **16**,  
468 (2015).
- 469 19. Liu, E. Y., Cali, C. P. & Lee, E. B. AT A GLANCE SPECIAL COLLECTION:  
470 NEURODEGENERATION RNA metabolism in neurodegenerative disease. (2017)  
471 doi:10.1242/dmm.028613.supplemental.
- 472 20. Johnson, J. O. *et al.* Mutations in the Matrin 3 gene cause familial amyotrophic lateral  
473 sclerosis. *Nat. Neurosci.* **17**, 664–666 (2014).
- 474 21. Marg, A. *et al.* Human satellite cells have regenerative capacity and are genetically  
475 manipulable. *J. Clin. Invest.* **124**, 4257–4265 (2014).
- 476 22. Peretti, D. *et al.* RBM3 mediates structural plasticity and protective effects of cooling in  
477 neurodegeneration. *Nature* **518**, 236–239 (2015).
- 478 23. Jackson, T. C. *et al.* Cold stress protein RBM3 responds to temperature change in an ultra-  
479 sensitive manner in young neurons. *Neuroscience* **305**, 268–278 (2015).
- 480 24. Ferry, A. L., Vanderklish, P. W. & Dupont-Versteegden, E. E. Enhanced survival of  
481 skeletal muscle myoblasts in response to overexpression of cold shock protein RBM3. *Am*  
482 *J Physiol Cell Physiol* **301**, 392–402 (2011).
- 483 25. Hettinger, Z. R., Confides, A. L., Vanderklish, P. W. & Dupont-Versteegden, E. E. The  
484 transcript interactome of skeletal muscle RNA binding protein motif 3 (RBM3). *Physiol.*  
485 *Rep.* **11**, (2023).
- 486 26. Zhou, Y. *et al.* Metascape provides a biologist-oriented resource for the analysis of  
487 systems-level datasets. *Nat. Commun.* **10**, (2019).
- 488 27. Li, Z. *et al.* The RNA-Binding Motif Protein Family in Cancer: Friend or Foe? *Frontiers*  
489 *in Oncology* vol. 11 (2021).

- 490 28. Garcia-Roves, P. M., Osler, M. E., Holmström, M. H. & Zierath, J. R. Gain-of-function  
491 R225Q mutation in AMP-activated protein kinase  $\gamma$ 3 subunit increases mitochondrial  
492 biogenesis in glycolytic skeletal muscle. *J. Biol. Chem.* **283**, 35724–35734 (2008).
- 493 29. Jä, S., Handschin, C., St.-Pierre, J. & Spiegelman, B. M. AMP-activated protein kinase  
494 (AMPK) action in skeletal muscle via direct phosphorylation of PGC-1. (2007).
- 495 30. Hawley, S. A. *et al.* Phosphorylation by Akt within the ST loop of AMPK- $\alpha$ 1 down-  
496 regulates its activation in tumour cells. *Biochem. J.* **459**, 275–287 (2014).
- 497 31. Aslam, M. & Ladilov, Y. Emerging Role of cAMP/AMPK Signaling. *Cells* vol. 11  
498 (2022).
- 499 32. Qin, X., Jiang, B. & Zhang, Y. 4E-BP1, a multifactor regulated multifunctional protein.  
500 *Cell Cycle* vol. 15 781–786 (2016).
- 501 33. Qin, S. *et al.* Pkm2 can enhance pluripotency in ESCs and promote somatic cell  
502 reprogramming to iPSCs.
- 503 34. Warden, S. M. *et al.* Post-translational modifications of the  $\beta$ -1 subunit of AMP-activated  
504 protein kinase affect enzyme activity and cellular localization. *Biochem. J* vol. 354 275–  
505 283 (2001).
- 506 35. Hong, X. *et al.* Mitochondrial dynamics maintain muscle stem cell regenerative  
507 competence throughout adult life by regulating metabolism and mitophagy. *Cell Stem Cell*  
508 **29**, 1298-1314.e10 (2022).
- 509 36. Apfeld, J., O’Connor, G., McDonagh, T., DiStefano, P. S. & Curtis, R. The AMP-  
510 activated protein kinase AAK-2 links energy levels and insulin-like signals to lifespan in  
511 *C. elegans*. *Genes Dev.* **18**, 3004–3009 (2004).
- 512 37. Curtis, R., O’Connor, G. & DiStefano, P. S. Aging networks in *Caenorhabditis elegans*:  
513 AMP-activated protein kinase (aak-2) links multiple aging and metabolism pathways.  
514 *Aging Cell* **5**, 119–126 (2006).
- 515 38. Onken, B. & Driscoll, M. Metformin induces a dietary restriction-like state and the  
516 oxidative stress response to extend *C. elegans* healthspan via AMPK, LKB1, and SKN-1.

- 517 *PLoS One* **5**, (2010).
- 518 39. Sousa-Victor, P., García-Prat, L. & Muñoz-Cánoves, P. Control of satellite cell function in  
519 muscle regeneration and its disruption in ageing. *Nature Reviews Molecular Cell Biology*  
520 vol. 23 204–226 (2022).
- 521 40. Hettinger, Z. R. *et al.* Skeletal muscle RBM3 expression is associated with extended  
522 lifespan in Ames Dwarf and calorie restricted mice. *Exp. Gerontol.* **146**, (2021).
- 523 41. Kar, M. *et al.* Phase-separating RNA-binding proteins form heterogeneous distributions of  
524 clusters in subsaturated solutions. (2022) doi:10.1073/pnas.
- 525 42. Bastide, A. *et al.* RTN3 Is a Novel Cold-Induced Protein and Mediates Neuroprotective  
526 Effects of RBM3. *Curr. Biol.* **27**, 638–650 (2017).

527

**Table 1**

CELLULAR PROCESSES	6 hrs	12 hrs	24 hrs	48 hrs
Metabolism of RNA	+	+	+	+
Cellular responses to stress	+	-	+	+
Monocarboxylic Acid metabolic processes	-	+	+	+
Amino Acid Metabolism	-	+	+	+
Acyl coA metabolic processes	-	-	+	+
Ribonucleotide metabolic processes	+	-	+	-
Regulation of splicing	+	-	+	-
Carbon metabolism	-	+	-	-

539 **Table 1** Summary of the GO enrichment pathway analysis of the cellular processes that were  
540 increased during hypothermia at different time points.

541

542

## 543 **Figure legends**

### 544 **Figure 1 Hypothermic adaptation (after 72 hrs.) enhances differentiation of skeletal muscle**

545 **cells. (A)** Schematic representing the hypothermia experiment where C2C12 myoblasts were  
546 differentiated into myotubes at 37<sup>0</sup>C after 72 hrs. of hypothermia (25<sup>0</sup>C or 32<sup>0</sup>C). **(B)** mRNA  
547 expression levels of Myosin heavy chain (*MyHC*) during differentiation using C2C12 cells at  
548 25<sup>0</sup>C and 37<sup>0</sup>C (n=3) where the x-axis represents the number of days pre-differentiation and  
549 during differentiation and the y-axis represents the mRNA fold change of *MyHC* normalized to  
550 18S rRNA and compared to D-2. **(C)** mRNA expression levels of *MyHC* during differentiation  
551 using C2C12 cells at 32<sup>0</sup>C and 37<sup>0</sup>C (n=3) where the x-axis represents the number of days pre-  
552 differentiation and during differentiation and the y-axis represents the mRNA fold change of  
553 *MyHC* normalized to 18S rRNA and compared to D-2. **(D)** mRNA expression levels of  
554 Myogenin (*Myog*) during differentiation in C2C12 cells at 25<sup>0</sup>C and 37<sup>0</sup>C (n=3) where the x-axis  
555 represents the number of days pre-differentiation and during differentiation and the y-axis  
556 represents the mRNA fold change of *Myog* normalized to 18S rRNA and compared to D-2. **(E)**  
557 mRNA expression levels of *Myog* during differentiation using C2C12 cells at 32<sup>0</sup>C and 37<sup>0</sup>C  
558 (n=3) where the x-axis represents the number of days pre-differentiation and during  
559 differentiation and the y-axis represents the mRNA fold change of *Myog* normalized to 18S  
560 rRNA and compared to D-2. **(F)** Western blot analysis of MyHC and MYOG during  
561 differentiation using C2C12 cells at 32<sup>0</sup>C and 37<sup>0</sup>C (n=2). The bar graph represents the  
562 MyHC/Actin and MYOG/Actin levels, where the x-axis represents the number of days pre-  
563 differentiation and during differentiation and the y-axis represents relative levels of MyHC and  
564 MYOG w.r.t to Actin. **(G)** Western blot analysis of MyHC and MYOG during differentiation  
565 using C2C12 cells at 25<sup>0</sup>C and 37<sup>0</sup>C (n=1). The bar graph represents the MyHC/Actin and  
566 MYOG/Actin levels, where the x-axis represents the number of days pre-differentiation and  
567 during differentiation and the y-axis represents relative levels of MyHC and MYOG w.r.t to  
568 Actin. **(H)** Western blot analysis of MyHC and MYOG during differentiation using mouse  
569 primary myoblasts at 32<sup>0</sup>C and 37<sup>0</sup>C (n=1). **(I)** mRNA expression levels of *MyHC* during  
570 differentiation using mouse primary myoblasts cells at 32<sup>0</sup>C and 37<sup>0</sup>C where the x-axis  
571 represents the number of days pre-differentiation and during differentiation and the y-axis

572 represents the mRNA fold change of *MyHC* normalized to 18S rRNA and compared to D-2. **(J)**  
573 mRNA expression levels of *Myog* during differentiation using mouse primary myoblasts at 32<sup>0</sup>C  
574 and 37<sup>0</sup>C where the x-axis represents the number of days pre-differentiation and during  
575 differentiation and the y-axis represents the mRNA fold change of *MyHC* normalized to 18S  
576 rRNA and compared to D-2. \*, \*\*, \*\*\* represent p-value < 0.05, 0.01 and 0.001 respectively.

577 **Figure 2 Proteomic mapping of the temporal response of C2C12 cells to hypothermia**  
578 **(32<sup>0</sup>C) at 6, 12, 24 and 48 hrs.** Heat map of upregulated proteins involved in **(A)** RNA  
579 metabolism and processing. **(B)** lipid metabolism. **(C)** TCA cycle. (n=3). Graph showing fold  
580 change of protein expression of RNA binding proteins **(D)** CIRBP **(E)** RBM3 during  
581 hypothermic treatment where the x-axis represents time in hours and the y-axis represents the  
582 relative fold change of the protein in hypothermic condition compared to control. **(F)** mRNA  
583 expression levels of *RBM3* using C2C12 cells at 32<sup>0</sup>C and 37<sup>0</sup>C at 72 hrs., where the x-axis  
584 represents the temperature, and the y-axis represents the mRNA fold change of RBM3  
585 normalized to 18S rRNA and compared to 37<sup>0</sup>C (n=3). **(G)** mRNA expression levels of RBM3  
586 using mouse primary myoblasts at 32<sup>0</sup>C and 37<sup>0</sup>C at 48 hrs. and 72 hrs. respectively, where the  
587 x-axis represents the temperature and the y-axis represents the mRNA fold change of *RBM3*  
588 normalized to 18S rRNA and compared to 37<sup>0</sup>C (n=2). **(H)** Western blot analysis of RBM3  
589 using C2C12 cells at 32<sup>0</sup>C and 37<sup>0</sup>C at 72 hrs. (n=2). **(I)** Western blot analysis of RBM3 using  
590 mouse primary myoblasts at 32<sup>0</sup>C and 37<sup>0</sup>C at 48 hrs. and 72 hrs. respectively (n=2).

591 **Figure 3 GO enrichment analysis of protein functional network of C2C12 cells in**  
592 **hypothermia (32<sup>0</sup>C) at 6, 12, 24 and 48 hrs.** GO enrichment protein functional network at **(A)**  
593 48 hrs. **(B)** 24 hrs. **(C)** 12 hrs. **(D)** 6 hrs. (n=3).

594 **Figure 4 RBM3 promotes differentiation and viability of skeletal muscle myoblasts.** **(A)**  
595 mRNA expression levels of *MyHC* for siRBM3 and scrambled control (scr) treatment using  
596 C2C12 cells at 32<sup>0</sup>C and 37<sup>0</sup>C (n=2), where the x-axis represents the number of days pre-  
597 differentiation and during differentiation and the y-axis represents the mRNA fold change of  
598 *MyHC* normalized to 18S rRNA and compared to D-2. **(B)** mRNA expression levels of *Myog*  
599 for siRBM3 and scrambled control (scr) treatment using C2C12 cells at 32<sup>0</sup>C and 37<sup>0</sup>C (n=2),  
600 where the x-axis represents the number of days pre-differentiation and during differentiation and  
601 the y-axis represents the mRNA fold change of *Myog* normalized to 18S rRNA and compared to

602 D-2. (C) mRNA expression levels of *MyHC* during differentiation using C2C12 cells  
603 overexpressing pMIG-GFP control and pMIG-RBM3 at 37<sup>0</sup>C (n=3), where the x-axis represents  
604 the number of days pre-differentiation and during differentiation and the y-axis represents the  
605 mRNA fold change of *MyHC* normalized to 18S rRNA and compared to D-2. (D) mRNA  
606 expression levels of *Myog* during differentiation using C2C12 cells overexpressing pMIG-GFP  
607 control and pMIG-RBM3 at 37<sup>0</sup>C (n=3), where the x-axis represents the number of days pre-  
608 differentiation and during differentiation and the y-axis represents the mRNA fold change of  
609 *Myog* normalized to 18S rRNA and compared to D-2. (E) Western blot analysis of MyHC and  
610 MYOG during differentiation using C2C12 cells overexpressing pMIG-GFP control and pMIG-  
611 RBM3 at 37<sup>0</sup>C (n=2). (F) mRNA expression levels of *MyHC* during differentiation using mouse  
612 primary myoblasts overexpressing pMIG-GFP control and pMIG-RBM3 at 37<sup>0</sup>C (n=2), where  
613 the x-axis represents the number of days pre-differentiation and during differentiation and the y-  
614 axis represents the mRNA fold change of *MyHC* normalized to 18S rRNA and compared to D-2.  
615 (G) mRNA expression levels of *Myog* during differentiation using mouse primary myoblasts  
616 overexpressing pMIG-GFP control and pMIG-RBM3 at 37<sup>0</sup>C (n=2), where the x-axis represents  
617 the number of days pre-differentiation and during differentiation and the y-axis represents the  
618 mRNA fold change of *Myog* normalized to 18S rRNA and compared to D-2. (H) Confocal  
619 images of C2C12 cells overexpressing pMIG-GFP control and pMIG-RBM3 at 37<sup>0</sup>C. Red  
620 indicates Ki-67 staining, blue indicates DAPI, and Green indicate GFP (Scale bar, 30um). (I) Bar  
621 graph representing the quantitation of Ki-67 staining where the y-axis represents the mean  
622 integrated density of Ki-67 positive nucleus stain. (J) Bar graph for MTT assay using C2C12  
623 cells overexpressing pMIG-GFP control and pMIG-RBM3 at 37<sup>0</sup>C where the Y axis represents  
624 absorbance at 570 nm (n=3). (K) Line graph indicating cell proliferation of C2C12 cells  
625 overexpressing pMIG-GFP control and pMIG-RBM3 at 37<sup>0</sup>C where the Y-axis represents the  
626 total number of cells and X-axis represents time in days (n=3). \*, \*\*, \*\*\* represents p-value <  
627 0.05, 0.01 and 0.001 respectively.

628 **Figure 5 Proteomic mapping of C2C12 cells overexpressing RBM3.** Heat map of upregulated  
629 proteins involved in (A) RNA metabolism and processing. (B) lipid metabolism. (C) ETC. (D)  
630 Venn diagram representing the upregulated proteins in 48 hrs. hypothermic treatment and RBM3  
631 overexpression and the common proteins between them in C2C12 cells. (E) GO enrichment  
632 pathway analysis of upregulated proteins in RBM3 overexpression (n=3).

633 **Figure 6 RBM3 promotes mitochondrial metabolism of skeletal muscle myoblasts.** (A)  
634 Graph showing the mitochondrial OCR of C2C12 cells overexpressing pMIG GFP and pMIG  
635 RBM3-GFP, basal OCR and OCR after treatment with oligomycin (1 uM), FCCP (3 uM),  
636 antimycin and rotenone (1.5 uM), where the x-axis represents time in minutes and the y-axis  
637 represents oxygen consumption rate in pMol/min. (B) Bar graph measuring the basal respiration,  
638 maximum respiration (OCR after FCCP addition), spare respiratory capacity (basal respiration-  
639 maximum respiration) and ATP-linked respiration (basal respiration-respiration after oligomycin  
640 addition) of C2C12 cells overexpressing pMIG-GFP and pMIG-RBM3 GFP where the y-axis  
641 represents oxygen consumption rate in pMol/Min (n=2). (C) Heat map showing levels of TCA  
642 metabolites using C2C12 cells overexpressing pMIG-GFP control and pMIG-RBM3. (D) Heat  
643 map showing levels of TCA metabolites using media (48 hrs.) from C2C12 cells overexpressing  
644 pMIG-GFP control and pMIG-RBM3 (n=3). (E) Graphical representation of levels of acetyl-  
645 CoA using C2C12 cells overexpressing pMIG-GFP control and pMIG-RBM3 (n=3). mRNA  
646 expression levels of glycolytic genes (F) *PKM1*, (G) *PKM2* in C2C12 overexpressing pMIG-  
647 GFP control and pMIG-RBM3. (H) Western blot analysis of glycolytic protein levels (PKM1,  
648 PKM2) using C2C12 cells overexpressing pMIG-GFP control and pMIG-RBM3. (I) mRNA  
649 expression levels of glycolytic genes *PKM1*, *PKM2* in mouse primary myoblasts overexpressing  
650 pMIG-GFP control and pMIG-RBM3 (n=3). (J) Western blot analysis of AMPK-beta and 4E-  
651 BP1 using C2C12 cells overexpressing pMIG-GFP control and pMIG-RBM3. (K) Western blot  
652 analysis of acetyl-CoA carboxylase (ACC) using C2C12 cells overexpressing pMIG-GFP control  
653 and pMIG-RBM3. (L) Bar graph quantifying phosphorylated/total 4E-BP1, ACC and AMPK-  
654 beta respectively. \*, \*\*, \*\*\* represents p-value < 0.05, 0.01 and 0.001 respectively.

655 **Figure 7: Overexpression of RBM3 increases stem cell markers in aged myoblasts.** mRNA  
656 expression levels of (A) *MyoD1* (B) *Pax7* (C) *Myf5* in aged myoblasts compared to young (D)  
657 mRNA expression levels of *MyHC* in aged myoblasts at 32<sup>o</sup>C compared to 37<sup>o</sup>C. (n=2) (E)  
658 mRNA expression levels of *RBM3* in aged myoblasts at 32<sup>o</sup>C compared to 37<sup>o</sup>C. mRNA  
659 expression levels of (F) *RBM3*, (G) *Pax7*, (H) *Myf5*, (I) *MyoD1* in aged myoblasts transfected  
660 with RBM3 and control GFP. (n=2 for all the mRNA studies) (J) Western blot analysis of  
661 MyoD1 using mouse primary myoblasts at proliferative stage (72 hrs. post-transfection)  
662 overexpressing RBM3-GFP and GFP control (n=2). \*, \*\*, \*\*\* represents p-value < 0.05, 0.01  
663 and 0.001 respectively.

664 **Figure 8:** Graphical representation showing the effect of mild hypothermia and RBM3  
665 overexpression on important cellular processes like RBM3 expression (1), RNA metabolism and  
666 splicing (2), translation (3) and mitochondrial metabolism (4) which finally leads to improved  
667 skeletal muscle regeneration.

668

## 669 **Materials and Methods**

### 670 **Cell culture techniques:**

671 C2C12 cells (purchased from ATCC) were grown and maintained in DMEM (Dulbecco's  
672 Modified Eagle Medium, Gibco-11995065) with 10% FBS (Foetal Bovine Serum, Gibco-  
673 16000044) and 1% Pen-Strep (Penicillin-Streptomycin, Gibco-15140122). Mouse primary  
674 myoblasts were cultured on ECM Gel coated dishes (Sigma-Aldrich-E6909). The cells were  
675 grown in 37<sup>0</sup>C and 5% CO<sub>2</sub> conditions. C2C12 differentiation was done using DMEM + 2%  
676 horse serum (Gibco-26050070) and 1% Pen-Strep. Differentiation media was added once the  
677 cells reach 100% confluency and differentiation was done for 6 days. HEK293T cells were  
678 grown and maintained in DMEM with 10% FBS and 1% Pen-Strep. For hypothermic stress,  
679 cells were grown in 25<sup>0</sup>C and 32<sup>0</sup>C and 5% CO<sub>2</sub> conditions for 72 hrs.

### 680 **Preparation of retrovirus and stable cell lines:**

681 For retrovirus production, HEK293T was cotransfected with the plasmid containing the gene of  
682 interest pMIG-GFP, pMIG-RBM3 and packaging plasmid pCL-ECO using jetPRIME reagent  
683 (Polyplus-101000046). Media was collected 48 hrs. and 72 hrs. after transfection. The collected  
684 media was centrifuged at 4000 RPM for 5 minutes at room temperature. The supernatant was  
685 collected and concentrated using Retro-X-Concentrator from Takara Biosciences (Takara  
686 #631455) overnight at 4<sup>0</sup>C. The following day the concentrate was centrifuged at 1500 RPM for  
687 45 minutes at 4<sup>0</sup>C to obtain the virus pellet. The pellet was resuspended in DMEM media and  
688 aliquoted and stored at -80<sup>0</sup>C if not used immediately.

689 The retroviral titre calculation was done using the Retroviral titration kit from Takara  
690 Biosciences (Retro-X™ qRT-PCR Titration Kit 631453) using the qRT-PCR-based method.

691 C2C12 cells were transduced with  $10^5$ - $10^6$  virus particles. C2C12 cells were seeded in a 6 cm  
692 dish and  $10^5$ - $10^6$  virus particles were added dropwise to media containing 8 ug/mL Sequabrene  
693 (Sigma S2667-1VL) and 25 mM Hepes buffer. The media was changed 24 hrs. after  
694 transduction. Cells were checked 48 hrs. after transduction and an efficiency of 90-95% was  
695 observed.

696

#### 697 **si-RNA treatment on C2C12 cells**

698 C2C12 cells were transfected with 200 nM of siRBM3 (Dharmacon L-041823-01-0005) and 200  
699 nM scrambled control (Dharmacon D-001810-10-05) using dharmafect transfection reagent  
700 following dharmefect transfection protocol.

701

#### 702 **Protein isolation and Western blotting:**

703 Protein isolation was done using RIPA buffer (Thermo Scientific-89901) and 1X PIC (Protease  
704 inhibitor cocktail cOmplete Roche 11697498001). The concentration of the protein was done  
705 using Bradford assay (Puregene PG-035-500mL) or BCA assay (G-Biosciences-786570). For  
706 western blotting 25 ug protein was loaded in each well. 3% BSA in TBST was used as a  
707 blocking buffer. Primary antibodies MyHC (Invitrogen 14650382), MF-20 (DHSB  
708 AB\_2147781) MYOG (Invitrogen MA5-11486), MyoD1 (Santa Cruz SC-377460), RBM3  
709 (Invitrogen PA5-51976), beta-ACTIN (CST 4967S), beta-Tubulin (CST 2146), PKM1(CST  
710 D30G6), beta-Actin (CST 4967 ) PKM2 (CST D78A4), PDH (CST 3205), SDHA (CST 5839),  
711 phospho-4E-BP1 (CST 2855), total 4E-BP1 (CST 9452), phospho-AMPK-alpha (CST 2535),  
712 total-AMPK-alpha (CST 5831), phospho-AMPK-beta (CST 4186), total-AMPK-beta (CST  
713 4150), phospho-ACC (CST 11818) and total ACC (CST 3676) were used in 1:1000 dilution and  
714 incubated at 4<sup>0</sup>C overnight. Secondary antibodies: anti-mouse IgG, HRP-linked (CST 7076) and  
715 anti-rabbit IgG, HRP-linked (CST 7074) were used in 1:5000 dilution and incubated at room  
716 temperature for 1hr. The blots were developed using a developing solution (advansta-K-12049-  
717 D50).

#### 718 **RNA isolation and qRT-PCR**

719 RNA isolation from cell samples was done using Trizol (Thermo Scientific-15596018). Reverse  
720 transcription was done using the TAKARA cDNA synthesis kit (PrimeScript™ 1<sup>st</sup> strand cDNA  
721 Synthesis Kit 6110A). qRT-PCR was done using SYBR-Green (PowerUp™ SYBR™ Green  
722 Master Mix A25742). Following primers were used for qRT:

723 *MyHC* (Forward primer: TAAACGCAAGTGCCATTCCTG, Reverse primer:  
724 GGGTCCGGGTAATAAGCTGG), *Myog* (Forward primer: CGATCTCCGCTACAGAGGC,  
725 Reverse primer: GTTGGGACCGAACTCCAGT), *MyoD1* (Forward primer:  
726 TCCGCTACATCGAAGGTCTG, Reverse primer: GTCCAGGTGCGTAGAAGGC), *rbm3*  
727 (Forward primer: CTTCGTAGGAGGGCTCAACTT, Reverse primer:  
728 CTCCCGGTCCTTGACAACAAC), 18S rRNA (Forward primer:  
729 CCCGTTGAACCCCATTCGTG, Reverse primer: GGGCCTCACTAAACCATCCA), *pkm1*  
730 (Forward primer: GCCGCCTGGACATTGACTC, Reverse primer:  
731 CCATGAGAGAAATTCAGCCGAG), *Pkm2* (Forward primer: CGCCTGGACATTGACTCTG,  
732 Reverse primer: GAAATTCAGCCGAGCCACATT), *Sdha* (Forward primer:  
733 GGAACACTCCAAAAACAGACCT, Reverse primer: CCACCACTGGGTATTGAGTAGAA),  
734 *Sdhc* (Forward primer: GCTGCGTTCTTGCTGAGACA, Reverse primer:  
735 ATCTCCTCCTTAGCTGTGGTT), *Pdhb* (Forward primer:  
736 AGGAGGGAATTGAATGTGAGGT, Reverse primer: ACTGGCTTCTATGGCTTCGAT) ,  
737 *Pax7* (Forward primer: CTCAGTGAGTTCGATTAGCCG, Reverse primer :  
738 AGACGGTTCCTTTGTCGC), *Myf5* (Forward primer: CACCACCAACCCTAACCAGAG,  
739 Reverse primer: AGGCTGTAATAGTTCTCCACCTG)

#### 740 **MTT assay**

741 For the MTT assay, 5 mg/mL MTT reagent was used (Sigma M2128-500MG). Cells were  
742 seeded in a 96-well plate. For drug assay, 10000 cells were seeded per well. The following day,  
743 cells were treated with drugs oligomycin (Sigma 75351) and 2DG (Sigma D8375) at different  
744 concentrations: 50 nM, 100 nM, and 200 nM for oligomycin and 0.25 mM, 0.5 mM, 1 mM for  
745 2DG for 48 hrs. After which cells were incubated with MTT reagent for 3 hrs. at 37°C in dark.  
746 Absorbance reading was taken at 570 nm using a plate reader. For the cell viability experiment,  
747 C2C12 stable lines: GFP, RBM3 have been seeded in 96 well plates 5,000 cells per well. MTT  
748 assay was done 48 hrs. after seeding and absorbance was measured at 570 nm.

## 749 **Seahorse Assay**

750 Seahorse assay was done to measure the oxygen consumption rate (OCR) of the cells using  
751 Seahorse XFe24 bioanalyser machine. For that, the 24 well cell culture plates (Agilent  
752 Technologies 102340-100) were seeded with 18000 cells per well. DMEM XF base media  
753 (Agilent 102353-100) containing 1 mM sodium pyruvate (Sigma S8636-100ML), 2 mM  
754 glutamine (Sigma G7513-100ML) and 20 mM glucose (Qualigens Q15405) for measuring OCR  
755 was used. Cells were incubated in a non-CO<sub>2</sub> incubator at 37<sup>0</sup>C for 45 minutes. OCR were  
756 measured in response to the following drugs: 1 uM oligomycin, 3 uM FCCP (Cayman chemical  
757 800364-9897), 1.5 uM of antimycin (Cayman chemicals 1397-94-0) and rotenone (Sigma  
758 R8875-1G) for OCR. Apart from the drug treatment, OCR was measured at the baseline levels.

## 759 **Proteomics sample extraction and preparation**

760 C2C12 cells were subjected to hypothermic conditions: 32<sup>0</sup>C and 5% CO<sub>2</sub> for different time  
761 points of 6 hrs., 12 hrs., 24 hrs., 48 hrs. C2C12 stable cell lines: GFP and RBM3 were used for  
762 proteomics studies. Cells were lysed with RIPA + Protease inhibitor cocktail. They were  
763 centrifuged at 10000 RPM for 30 minutes at 4<sup>0</sup>C. The supernatant was collected, and a BCA  
764 assay was done. 100 ug of protein was used for proteomic analysis. Chilled acetone was added to  
765 the protein samples and incubated for 3 hrs. at -80<sup>0</sup>C. Centrifugation was done at 13,000 RPM  
766 for 30 minutes at 4<sup>0</sup>C. The pellet was washed with acetone at 13000 RPM for 10 minutes at 4<sup>0</sup>C.  
767 The samples were treated with 8 M urea (in Ammonium bicarbonate) and 0.5 M DTT and  
768 incubated for 30 minutes at 37<sup>0</sup>C. Following this, the samples were treated with 30 mM  
769 iodoacetamide and incubated for 30 minutes at 37<sup>0</sup>C. The samples were then digested with  
770 trypsin (1:20 trypsin: protein) at 37<sup>0</sup>C overnight. The digested samples were desalted using the  
771 C18 column. The column was equilibrated with 0.1% formic acid. The sample was eluted in  
772 100% Acetonitrile containing 0.1% formic acid. The eluted samples were dried using a speed  
773 vacuum.

## 774 **Separation and digested protein for Identification and quantitation of the Proteome using** 775 **Sciex 7600 Zeno-TOF LCMS:**

776 Equal concentrations of protein samples were digested using mass spec grade trypsin and  
777 digested peptides were desalted using a C18 SPE cartridge. Peptides were analyzed using a Sciex

778 Zeno TOF 7600 (AB Sciex, Foster City, CA, United States) equipped with a Shimadzu LC 40  
779 UPLC system. Peptides were separated on Aquity UPLC BEH C18 column (150 × 1 mm, 1.7  
780 μm,) column using a gradient of water and acetonitrile. For protein quantitation, spectral libraries  
781 were generated using information-dependent acquisition (IDA) mode after injecting 3 μg of  
782 tryptic digest on the above-mentioned C18 column using a Shimadzu LC40 autosampler system  
783 coupled with Sciex Zeno Tof 7600 fitted. For library generation, the peptides from all the  
784 experiment sets were pooled and injected into the mass spec for comprehensive coverage. The  
785 total chromatography run time was 180 minutes. The first 10 minutes of the column flow was  
786 sent to waste after loading for online desalting of the sample. A 180 minutes gradient in multiple  
787 steps (ranging from 5 to 30% acetonitrile in water containing 0.1% formic acid) was set up to  
788 elute the peptides from the column for the first 135 minutes then in the next 10 minutes  
789 concentration of B was increased to 55% and most of the peptide eluted till this time of 145  
790 minutes. The concentration of mobile phase B was increased to 95% B in 6 minutes and held at  
791 this concentration for 5 minutes then the column was again kept at 98% of mobile phase A  
792 (Water and 0.1% formic acid) for 24 minutes for equilibration. The flow rate of the UPLC was  
793 set at 30μL/minutes. Three biological replicates of the samples were run for each experimental  
794 set. For library preparation the mass spec was run in an information-dependent acquisition mode  
795 (IDA) with the MS1 mass range of 350 Da to 1500 Da, Gas 1 was 25 L/min, Gas 2 was set at 15  
796 L/minutes, whereas curtain gas was set at 25 L/minutes, ionization voltage was 5500 volt,  
797 accumulation time was set at 0.2 seconds and source temperature was at 350°C. The most  
798 abundant top 50 multiple charge precursor was fragmented in each cycle with dynamic collision  
799 energy in collision-induced dissociation (CID). The mass range for MS/MS was set at 150 to  
800 1800 Da. Zeno trapping was on for the IDA data.

### 801 **Sequential Window Acquisition of all Theoretical Fragment Ion Spectra (SWATH)** 802 **Analysis for Label-Free Quantification**

803 For label-free quantification (SWATH analysis) the Q1 transmission windows were set to 25 Da  
804 from the mass range of 350 Da to 1500 Da. A total of 79 windows were acquired independently  
805 with an accumulation time of 50 milliseconds. The total cycle time was kept constant at 2  
806 seconds. Protein Pilot™ v. 5.0.2 was used to generate the spectral library. For label-free  
807 quantification, peak extraction and spectral alignment were performed using PeakView<sup>R</sup>

808 2.2.0.11391 Software with the parameters set as follows: number of peptides, 2; number of  
809 transitions, 5; peptide confidence, 95%; XIC width, 20 ppm; XIC extraction window, 5 minutes.  
810 The data were further processed in MarkerView software<sup>TM</sup>. 1.3.1 (AB Sciex, Foster City, CA,  
811 United States) for statistical data interpretation. In MarkerView<sup>TM</sup>, the peak areas under the  
812 curve (AUC) for the selected transition were normalized using total area sum intensities and all  
813 the biological replicates were averaged out before normalization. t-test was performed on the  
814 data set and fold-changed values were calculated for all the proteins.

### 815 **Data Analysis for proteomics**

816 Data were processed with Protein Pilot Software v. 5.0.2 (ABSciex, Foster City, CA, United  
817 States) utilizing the Paragon and Progroup Algorithm. The analysis was done using the tools  
818 integrated into Protein Pilot at a 1% false discovery rate (FDR) with statistical significance. In  
819 brief, the UniProt mouse proteome database (UP000000589) was used to search for the matched  
820 peptide for library generation. The download included total combined (reviewed and un-  
821 reviewed) entries of 55,286 proteins. The resultant search identification file was used as a library  
822 for the extraction of peptide quantitation information from the SWATH acquisition. The  
823 extracted peptide information was processed using Marker view software<sup>TM</sup>(V1.3) for statistical  
824 analysis. Biological triplicate data for each sample were normalized using the total area sum  
825 method and all the biological replicates were averaged out for the calculation of fold change  
826 calculation. After normalization t-test and principal component analysis were performed on the  
827 data set to check the possible correlated variables within the group. A volcano plot was  
828 generated to calculate the statistically significant fold change vs p-value. Proteins with less than  
829 0.8-fold change were considered as downregulated and proteins with more than 1.5 fold change  
830 were considered as upregulated in the experiment sets. In this analysis library was made for  
831 approximately 2394 proteins that were identified with 0.05% False Discovery Rate (FDR) and  
832 approximately 1400 proteins were quantified in the data set. GO enrichment analysis, process  
833 and pathway enrichment analysis were done using metascap software.

### 834 **Metabolite Extraction and mass spectrometry**

835 C2C12 stable lines-GFP, RBM3 were seeded in 10 cm cell culture dishes. Metabolite extraction  
836 was done using chilled 50% methanol<sup>43</sup>. The cells were scrapped in 50% methanol and 100 ug  
837 D4 alanine (Cambridge isotope lab DLM-250-1) and centrifuged at 13000 RPM for 5 minutes at

838 room temperature. The supernatant was dried using a speed vacuum. The dried sample was  
839 stored at  $-80^{\circ}\text{C}$ . The pellet was resuspended in RIPA and protein was prepared and a BCA assay  
840 was done to determine the concentration. The media from the cells were processed similarly  
841 using 50% methanol. The dried samples were reconstituted and run on AB Sciex 5500 using the  
842 Synergi rp fusion column.

843 For the detection of glycolytic and pentose phosphate pathway intermediates along with NAD,  
844 NADH, and acetyl-CoA, the samples were analysed in a triple-quadrupole type mass  
845 spectrometer (Sciex QTRAP 5500) with Schmadzu HPLC unit. Multiple reaction monitoring  
846 (MRM) methods were modified as published by \*Walvekar et al\* (2018)  
847 The metabolites were measured using Synergi, 4  $\mu\text{m}$  Fusion-RP 80 A (150 x 2 mm; Phenomenex  
848 # 00F-4424-B0) by the methods described below:  
849 Samples were reconstituted in 100  $\mu\text{l}$  of 50% methanol.  
850 Synergi, 4  $\mu\text{m}$  Fusion-RP 80 A (150 x 2 mm; Phenomenex # 00F-4424-B0)  
851 Pump B; 0 minute: 0%; 2.0 minutes: 5%; 6.7 minutes: 60%; 7.3 minutes: 95%; 9.3 minutes:  
852 95%; 10 minutes: 5%; 10.3 minutes: 0%; 12 minutes: 0%; 12.1 minutes: controller stop; flow  
853 rate 0.2 ml/minutes; autosampler temperature  $5^{\circ}\text{C}$ ; Mobile phase A: 5mM Ammonium Acetate  
854 (Sigma 73594-25G-F) pH 8.0; Mobile phase B:100% acetonitrile (Fischer Scientific A955-4)  
855

856 The area under each peak was calculated using AB SCIEX MultiQuant software 3.0.1  
857

858 For TCA intermediates along with lactate and pyruvate, the mobile phase consisted of a  
859 premixed ratio of Water/Methanol (95:5) with 0.2 % Formic acid. The column heating oven was  
860 set to  $45^{\circ}\text{C}$ , autosampler temperature  $5^{\circ}\text{C}$ ; flow rate 0.4 mL/minutes.  
861 The MS method was used as such as per the manufacturer's instruction (Phenomenex TN-1241).

## 862 **Lipidomics sample preparation and analysis**

863 C2C12 stable lines-GFP, RBM3 were seeded in a 6 cm dish. Lipid extraction was done using the  
864 SIMPLEX protocol <sup>44</sup>. 225  $\mu\text{L}$  of methanol containing 10  $\mu\text{L}$  SPLASH LIPIDOMIX standard  
865 (Avanti polar lipids 330707) was added to the cell pellet and transferred to lo-bind Eppendorf  
866 tubes. The tubes were vortexed for 20 seconds and incubated in liquid nitrogen for 1 minute. It  
867 was then thawed at room temperature and sonicated for 30 minutes. 750  $\mu\text{L}$  of MTBE (Sigma

868 650560) was added to the vials and vortexed for 1 hr. at 4<sup>0</sup>C. 188 uL of water was added to  
869 induce phase separation after which centrifugation was done at 10,000g for 5 minutes at 4<sup>0</sup>C.  
870 The upper phase (600 uL) was collected for lipidomics. The solvent was dried and resuspended  
871 in 200 uL of solvent B (10 mM ammonium formate, 0.1% formic acid in 90:10, 2-Propanol:  
872 acetonitrile). For the liquid chromatography separation, mobile phase A was water/acetonitrile  
873 (60/40, v/v) and mobile phase B was 2-propanol/acetonitrile (90/20, v/v), with both containing  
874 10 mM ammonium formate and 0.1% formic acid. A 5 uL sample, thermostatted to 10<sup>0</sup>C, was  
875 injected onto a Thermo Scientific, Acclaim C30, reversed phase column (3 μm, 2.1 X 100 mm)  
876 thermostatted to 40<sup>0</sup>C in a Thermo Vanquish UHPLC system. Gradient elution was performed at  
877 a flow rate of 300 μL/minutes, beginning with 20% mobile phase B, that was increased to 40% B  
878 over 1 minutes, to 80% B over 8 minutes, to 100% B over 11 minutes, and held at 100% B until  
879 12 minutes, the column was re-equilibrated at 20% mobile phase B from 13 minutes to 15  
880 minutes, giving a total run time of 15 minutes. The lipidomic analysis was performed on a  
881 quadrupole-orbitrap mass spectrometer (Q Exactive, Thermo Fisher Scientific) operating in  
882 positive ion mode via electrospray ionization and used to scan from m/z 150 to 1000 at 1 Hz and  
883 140,000 resolution. Data were analyzed using the Lipid Search software.

884

### 885 **Immunofluorescence and confocal microscopy**

886 C2C12 cells were seeded on coverslips and subjected to hypothermia (32<sup>0</sup>C) and control (37<sup>0</sup>C)  
887 for 72 hrs. Cells were fixed with 4% PFA for 15 minutes at room temperature. Permeabilization  
888 was done using 0.1% triton-X-100 in 1X-PBS for 10 minutes at room temperature. Blocking was  
889 done for 1 hr. using 5% BSA in PBST at room temperature. Primary antibody (RBM3, Ki-67  
890 (Invitrogen PA5-19462)) was used at a dilution of 1:300 and incubated at 4<sup>0</sup>C overnight. The  
891 secondary antibody Alexa fluor 647 goat anti-rabbit (Invitrogen A21245) was used at 1:500  
892 dilution for 1 hr. at room temperature. For nuclear staining, DAPI (Thermo Scientific 62248)  
893 was used at a dilution of 1:1000 for 5 minutes. Coverslips were mounted using Prolong gold  
894 mounting agent (Life technologies P36930). Images were taken using a confocal microscope.

895

### 896 **Mitotracker and TMRM staining**

897 C2C12 stable lines-GFP, RBM3 were seeded in imaging dishes. After 24 hrs., the cells were  
898 stained with mitotracker (Invitrogen M7512) for 15 minutes at 37<sup>0</sup>C. The cells were washed with  
899 PBS. For nuclear staining, cells were incubated with Hoechst (Invitrogen H3570) (1:1000) for 5  
900 minutes and cells were imaged using a confocal microscope. For TMRM staining, cells were  
901 incubated with TMRM (Sigma T5428-25MG) stain for 10 minutes at 37<sup>0</sup>C and Hoechst for 5  
902 minutes and imaged using a confocal microscope.

### 903 **Neon transfection**

904 Mouse primary myoblasts were transfected with pMIG-RBM3 and pMIG-GFP using the Neon  
905 TM transfection system (Invitrogen MPK 1025). The cells were trypsinized and counted using a  
906 hemocytometer. For 12 well plate 3,00,000 cells and 2 ug DNA was used for transfection. The  
907 cell pellet was resuspended in 10 uL Buffer R and DNA was added to it. The cell suspension  
908 with DNA was placed on the neon tube containing 3mL of Buffer E and the electroporation was  
909 performed using the transfection program. The parameters used for transfection are voltage:  
910 1500V, pulse width: 10 milliseconds , no of pulse:3. The cells were grown without antibiotics for  
911 48 hrs. after transfection. After 48 hrs. cells were grown in growth media containing antibiotics.

### 912 **Satellite cell isolation and growth techniques**

913 Satellite cells were isolated from young (3-4 months) and aged (18 months) BL6/J mice using  
914 the Miltenyi satellite cell isolation kit (Miltenyi biotech 130-104-268). Due to the low viability  
915 of cells using the kit-based method, a non-kit-based method was used to isolate satellite cells  
916 from aged mice<sup>45</sup>. Before seeding, the tissue culture dishes were coated with ECM.

### 917 **Cloning techniques**

918 Mouse RBM3 gene from RBM3-PUC plasmid (Origene MC203679) was cloned into pMIG-  
919 GFP plasmid by restriction digestion method using Bgl2 and EcoR1 (NEB). Primers used for  
920 cloning (Forward primer: GGAAGATCTTATGTCGTCTGAAGAAGGGAAACTC, Reverse  
921 primer: CCGGAATTCTCAGTTGTCATAATTGTCTCT). ΔRBD was created by deleting 143  
922 bp from the N terminus of the RBM3 sequence. ΔRBD was cloned into pMIG-GFP plasmid by  
923 restriction digestion method using Bgl2 and EcoR1 using the following primers: Forward primer:  
924 GGAAGATCtATGTTTGGCTTCATCACC , Reverse primer:  
925 CCGGAATTCTCAGTTGTCATAATTGTC. The clone sequences were verified using the

926 Sanger sequencing technique. All the plasmids were purified using Qiagen miniprep kit (Qiagen  
927 27104). For neon transfection of primary myoblasts, RBM3-GFP plasmid from Origene was  
928 used (Origene MG201130).

### 929 **Statistical Analysis**

930 All the data are represented as mean  $\pm$  SEM. All the bar graphs were generated using graph pad  
931 Prism 8 using unpaired t-test or two-way ANOVA using multiple comparisons. Statistical  
932 significance was accepted at  $p \leq 0.05$

### 933 **Method references**

934 43. Walvekar, A., Rashida, Z., Maddali, H. & Laxman, S. A versatile LC-MS/MS approach  
935 for comprehensive, quantitative analysis of central metabolic pathways [version 1;  
936 referees: 2 approved]. *Wellcome Open Res.* **3**, (2018).

937 44. Coman, C. *et al.* Simultaneous metabolite, protein, lipid extraction (SIMPLEX): A  
938 combinatorial multimolecular omics approach for systems biology. *Mol. Cell. Proteomics*  
939 **15**, 1453–1466 (2016).

940 45. Benedetti, A. *et al.* A novel approach for the isolation and long-term expansion of pure  
941 satellite cells based on ice-cold treatment. *Skelet. Muscle* **11**, (2021).

### 942 **Acknowledgements**

943 The authors would like to acknowledge funding from the Department of Biotechnology, Govt of  
944 India. PD was funded by the CSIR fellowship, SM was funded by the DBT-RA fellowship. We  
945 thank Prof. Apurva Sarin for pMIG-GFP plasmid.

### 946 **Author Contributions:**

947 PD contributed to the cell culture, molecular biology, biochemical assays and writing of the  
948 manuscript. SR and PST contributed to the cell culture and molecular biology work. NS and PS  
949 contributed to western blot analysis. MAH performed metabolomic analysis. SM, RGHM  
950 performed Lipidomic analysis, HL and SSP performed confocal imaging. NS contributed to the  
951 proteomic studies. AR participated in the conceptualization and writing of the manuscript.

952 **Competing Interest Statement:** The authors do not have any competing interests.

953

#### 954 **Data sharing plans**

955 All raw data including mass spectrometry data will be shared in publicly available databases  
956 upon publication. All the mass spec raw and processed data file will be uploaded on the  
957 Proteomics identification database (PRIDE) for review and accessibility. Other data file of the  
958 experiment will also be available as made available for review.

#### 959 **Additional information**

960 Supplementary information is available for this paper

961 †All correspondence addressed to Arvind Ramanathan

962 **Email:** [arvind@instem.res.in](mailto:arvind@instem.res.in)

963

964

#### 965 **Supplementary figure legends**

966 **Supplementary 1 (A)** mRNA expression levels of Myosin heavy chain (*MyHC*) during  
967 differentiation using C2C12 cells at 25<sup>0</sup>C and 32<sup>0</sup>C compared to each other after 72 hrs. of  
968 hypothermic adaptation where the x-axis represents the number of days pre-differentiation and  
969 during differentiation and the y-axis represents the mRNA fold change of *MyHC* **(B)**  
970 Representative images of C2C12 myoblasts taken under bright field microscope at 10X. (Scale  
971 bar, 50 um) and myotubes (Scale bar, 100 um).

972 **Supplementary 2 (A)** Heat map of upregulated proteins involved in mitochondrial and fatty acid  
973 metabolism at different time points of 6 hrs., 12 hrs., 24 hrs. and 48 hrs. (n=3). **(B)** Heat map of  
974 upregulated proteins involved in RNA processing and metabolism at different time points of 6  
975 hrs., 12 hrs., 24 hrs. and 48 hrs. (n=3). **(C)** Volcano plot of 37<sup>0</sup>C compared to 32<sup>0</sup>C hypothermia  
976 at 6 hrs., 12 hrs., 24 hrs., 48 hrs., RBM3 overexpressed and GFP control where x-axis represents  
977 p-value and y-axis represents log (fold change).

978 **Supplementary 3 (A)** Bar graph representing the total number of upregulated and  
979 downregulated proteins and % of upregulated and downregulated proteins at different time points

980 of 6 hrs., 12 hrs., 24 hrs. and 48 hrs. at 32<sup>0</sup>C. GO enrichment pathway analysis of upregulated  
981 proteins at (B) 6 hrs. (C) 12 hrs. (D) 24 hrs. and (E) 48 hrs. at 32<sup>0</sup>C as analyzed by metascap.

982

983 **Supplementary 4 (A)** Western blot analysis of RBM3 using different concentrations of siRBM3  
984 in C2C12 cells at 37<sup>0</sup>C for 72 hrs. (B) mRNA expression levels of RBM3 using C2C12 cells  
985 overexpressing pMIG-GFP control, pMIG-RBM3 at 37<sup>0</sup>C (n=2). (C) mRNA expression levels of  
986 *MyoD1* in mouse primary myoblasts transfected with pMIG-RBM3 and pMIG-GFP (n=2). (D)  
987 Representative images of stable C2C12 cells transduced with pMIG-RBM3 in bright field and  
988 epifluorescence (Scale bar, 100 um) (E) Epifluorescence images of C2C12 transfected with  
989 RBM3-GFP taken at 100X (oil) (Scale bar, 16 um). \*, \*\*, \*\*\* represents p-value < 0.05, 0.01  
990 and 0.001 respectively.

991 **Supplementary 5 (A)** GO enrichment analysis of protein functional network of proteins  
992 upregulated in C2C12 cells overexpressing RBM3 analyzed by Metascap.

993 **Supplementary 6 (A)** Bar graph showing the % viability of C2C12 cells overexpressing pMIG-  
994 GFP, pMIG-RBM3 in presence of different concentrations of oligomycin (50 nM, 100 nM and  
995 200 nM) (B) IC50 plot for oligomycin using C2C12 cells overexpressing pMIG-GFP control and  
996 pMIG-RBM3 where the x-axis represents the oligomycin concentration and the y-axis represents  
997 the % viability of the cells (n=2). (C) Bar graph showing the % viability of C2C12 cells  
998 overexpressing pMIG-GFP control, pMIG-RBM3 in presence of different concentrations of  
999 2DG. (D) IC50 plot for 2DG using C2C12 cells overexpressing pMIG-GFP control and pMIG-  
1000 RBM3 where the x-axis represents the oligomycin concentration and the y-axis represents the %  
1001 viability of the cells (n=2). \*, \*\*, \*\*\* represents p-value < 0.05, 0.01 and 0.001 respectively.

1002 **Supplementary 7 (A)** Confocal images of C2C12 cells overexpressing pMIG-GFP control and  
1003 pMIG-RBM3. Red indicates mitotracker (100 mM), blue indicates Hoescht and green indicates  
1004 GFP (Scale bar, 16 um) (B) Confocal images of C2C12 cells overexpressing pMIG-GFP control  
1005 and pMIG-RBM3. Red indicates TMRM, blue indicates Hoescht and green indicates GFP (Scale  
1006 bar, 16 um) (C) Western blot analysis of SDHA and PDH using C2C12 cells overexpressing  
1007 pMIG-GFP control and pMIG-RBM3 (D) mRNA expression levels of *Sdha*, *Sdhc* and *Pdhh*  
1008 using C2C12 cells overexpressing pMIG-GFP control and pMIG-RBM3 (n=4). (E) mRNA

1009 expression levels of *Sdha*, *Sdhc* and *Pdhb* using mouse primary myoblasts overexpressing  
1010 pMIG-GFP control and pMIG-RBM3 (n=3). **(F)** Heat map showing levels of lactate/pyruvate  
1011 using C2C12 cells overexpressing pMIG-GFP control and pMIG-RBM3 (n=3). **(G)** Heat map  
1012 showing levels of lactate/pyruvate using media from C2C12 cells (48 hrs.) overexpressing  
1013 pMIG-GFP control and pMIG-RBM3 (n=3). **(H)** Western blot analysis of AMPK-alpha using  
1014 C2C12 cells overexpressing pMIG-GFP control and pMIG-RBM3 **(I)** Bar graph quantifying the  
1015 levels of phosphorylated/total AMPK-alpha. \*, \*\*, \*\*\* represents p-value < 0.05, 0.01 and  
1016 0.001 respectively.

1017 **Supplementary 8** Volcano plot of **(A)** Intracellular metabolites of C2C12 cells overexpressing  
1018 GFP and RBM3 **(C)** Extracellular metabolites of C2C12 cells overexpressing GFP and RBM3  
1019 where the x-axis represents the log of fold change and the y-axis represents -log of p-value .  
1020 Grey dots represent non-significant metabolite species and blue dot represents significantly high  
1021 levels of metabolite species (n=3). Heat map showing levels of TCA metabolites using C2C12  
1022 cells overexpressing pMIG-GFP control and pMIG-RBM3 **(B)** intracellular **(C)** extracellular  
1023 (n=3). \*, \*\*, \*\*\* represents p-value < 0.05, 0.01 and 0.001 respectively.

1024 **Supplementary 9** **(A)** Volcano plot of GFP and RBM3 overexpression where the x-axis  
1025 represents the log of fold change and the y-axis represents -log of p-value . Grey dots represent  
1026 non-significant lipid species and blue dot represents significantly low levels of lipid species  
1027 (n=3). **(B)** Heat map showing levels of cholesterol esters and triglycerides using C2C12 cells  
1028 overexpressing pMIG-GFP control and pMIG-RBM3 (n=3). \*, \*\*, \*\*\* represents p-value <  
1029 0.05, 0.01 and 0.001 respectively.

1030 **Supplementary 10** mRNA expression levels of **(A)** *MyHC* and **(B)** *Myog* of aged and young  
1031 myoblasts (n=3). **(C)** mRNA expression levels of *Myog* of aged myoblasts at 32<sup>0</sup>C compared to  
1032 37<sup>0</sup>C (n=2). **(D)** Bar graph showing the comparative  $\Delta$ Ct values of young primary, aged primary  
1033 and aged primary transfected with RBM3-GFP (n=2). Heat map showing levels of extracellular  
1034 lactate/pyruvate ratio **(E)** 24 hrs. **(F)** 48 hrs. and TCA metabolites in aged mouse primary  
1035 myoblasts transfected with RBM3-GFP and GFP control **(G)** 24 hrs. **(H)** 48 hrs. (n=3). \*, \*\*,  
1036 \*\*\* represents p-value < 0.05, 0.01 and 0.001 respectively.

1037 **Supplementary 11** **(A)** Representative images of mouse primary myoblasts (young and aged)  
1038 and differentiated cells (Scale bar, 100 um) **(B)** Representative images of mouse primary young

1039 myoblasts transfected with pMIG-RBM3 and pMIG-GFP in bright field and epifluorescence  
1040 (Scale bar, 100 um).

**Figure 1**

bioRxiv preprint doi: <https://doi.org/10.1101/2023.05.05.539524>; this version posted May 5, 2023. The copyright holder for this preprint (which was not certified by peer review) is the author/funder, who has granted bioRxiv a license to display the preprint in perpetuity. It is made available under aCC-BY-NC-ND 4.0 International license.

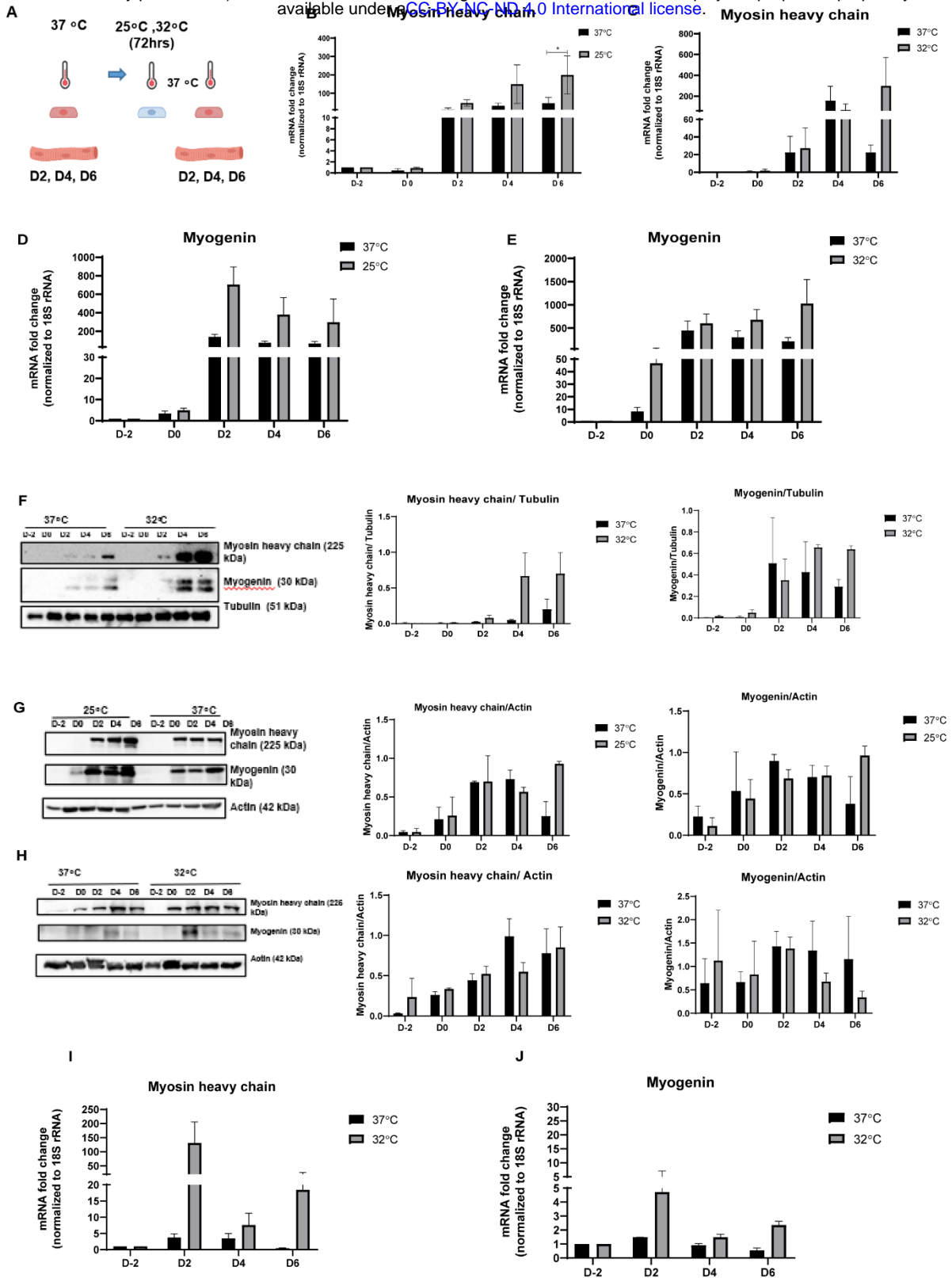


**Figure 1 Hypothermic adaptation (after 72 hrs.) enhances differentiation of skeletal muscle cells. (A) Schematic representing the hypothermia experiment where C2C12 myoblasts**

were differentiated into myotubes at 37°C after 72 hrs. of hypothermia (25°C or 32°C). **(B)** mRNA expression levels of Myosin heavy chain (*MyHC*) during differentiation using C2C12 cells at 25°C and 37°C (n=3) where the x-axis represents the number of days pre-differentiation and during differentiation and the y-axis represents the mRNA fold change of *MyHC* normalized to 18S rRNA and compared to D-2. **(C)** mRNA expression levels of *MyHC* during differentiation using C2C12 cells at 32°C and 37°C (n=3) where the x-axis represents the number of days pre-differentiation and during differentiation and the y-axis represents the mRNA fold change of *MyHC* normalized to 18S rRNA and compared to D-2. **(D)** mRNA expression levels of Myogenin (*Myog*) during differentiation in C2C12 cells at 25°C and 37°C (n=3) where the x-axis represents the number of days pre-differentiation and during differentiation and the y-axis represents the mRNA fold change of *Myog* normalized to 18S rRNA and compared to D-2. **(E)** mRNA expression levels of *Myog* during differentiation using C2C12 cells at 32°C and 37°C (n=3) where the x-axis represents the number of days pre-differentiation and during differentiation and the y-axis represents the mRNA fold change of *Myog* normalized to 18S rRNA and compared to D-2. **(F)** Western blot analysis of MyHC and MYOG during differentiation using C2C12 cells at 32°C and 37°C (n=2). The bar graph represents the MyHC/Actin and MYOG/Actin levels, where the x-axis represents the number of days pre-differentiation and during differentiation and the y-axis represents relative levels of MyHC and MYOG w.r.t to Actin. **(G)** Western blot analysis of MyHC and MYOG during differentiation using C2C12 cells at 25°C and 37°C (n=1). The bar graph represents the MyHC/Actin and MYOG/Actin levels, where the x-axis represents the number of days pre-differentiation and during differentiation and the y-axis represents relative levels of MyHC and MYOG w.r.t to Actin. **(H)** Western blot analysis of MyHC and MYOG during differentiation using mouse primary myoblasts at 32°C and 37°C (n=1). **(I)** mRNA expression levels of *MyHC* during differentiation using mouse primary myoblasts cells at 32°C and 37°C where the x-axis represents the number of days pre-differentiation and during differentiation and the y-axis represents the mRNA fold change of *MyHC* normalized to 18S rRNA and compared to D-2. **(J)** mRNA expression levels of *Myog* during differentiation using mouse primary myoblasts at 32°C and 37°C where the x-axis represents the number of days pre-differentiation and during differentiation and the y-axis represents the mRNA fold change of *MyHC* normalized to 18S rRNA and compared to D-2. \*, \*\*, \*\*\* represent p-value < 0.05, 0.01 and 0.001 respectively.

**Figure 2**

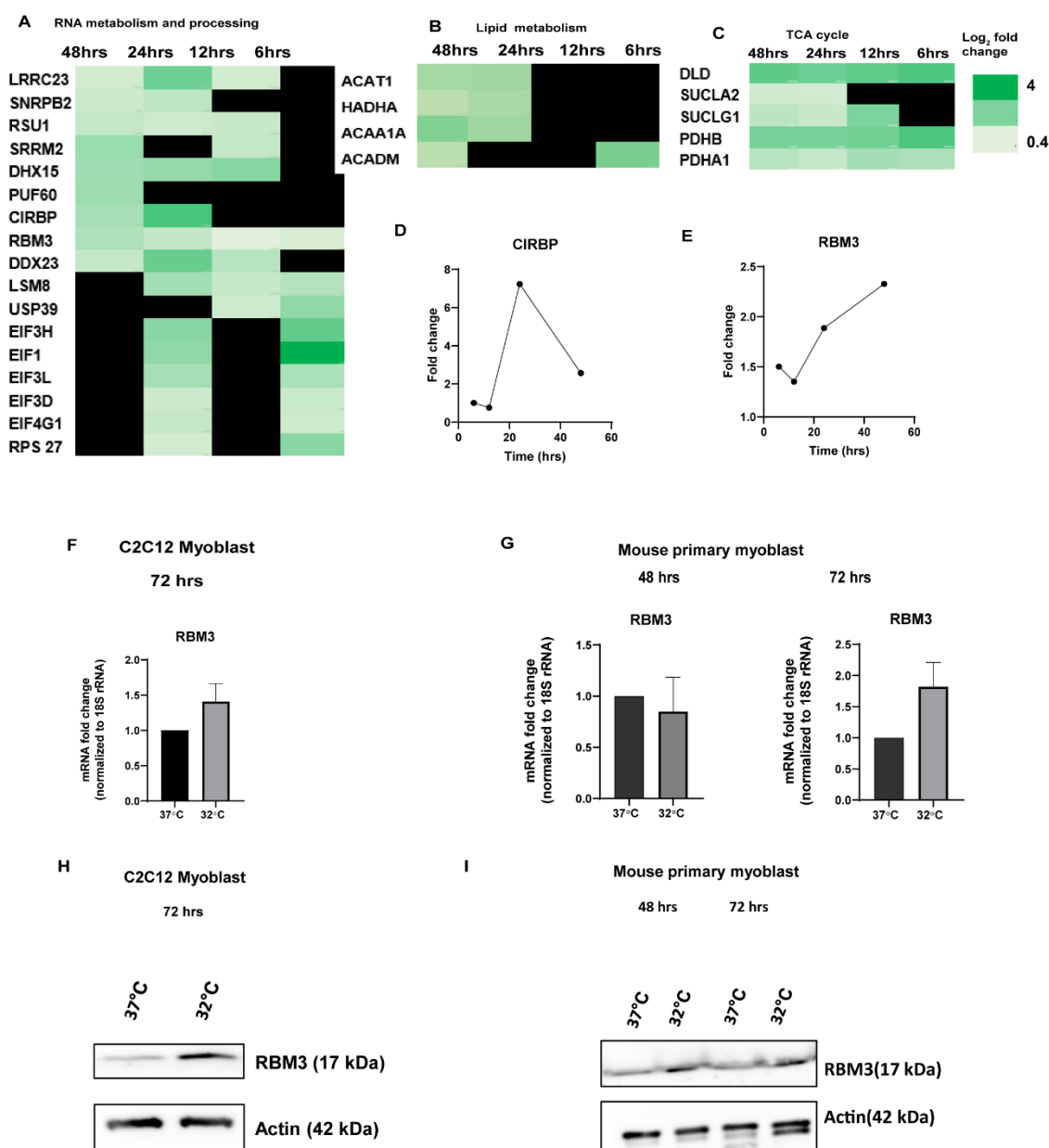


**Figure 2 Proteomic mapping of the temporal response of C2C12 cells to hypothermia (32°C) at 6, 12, 24 and 48 hrs.** Heat map of upregulated proteins involved in (A) RNA metabolism and processing. (B) lipid metabolism. (C) TCA cycle. (n=3). Graph showing fold change of protein expression of RNA binding proteins (D) CIRBP (E) RBM3 during

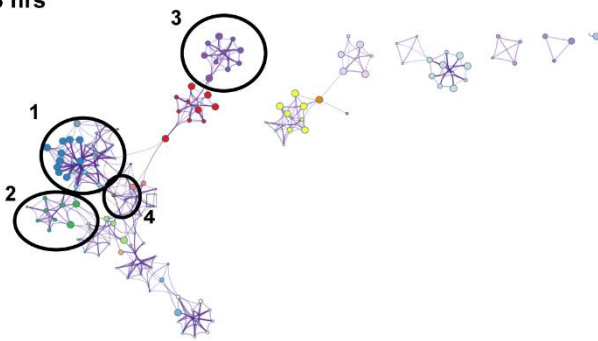
hypothermic treatment where the x-axis represents time in hours and the y-axis represents the relative fold change of the protein in hypothermic condition compared to control. **(F)** mRNA expression levels of *RBM3* using C2C12 cells at 32<sup>0</sup>C and 37<sup>0</sup>C at 72 hrs., where the x-axis represents the temperature, and the y-axis represents the mRNA fold change of *RBM3* normalized to 18S rRNA and compared to 37<sup>0</sup>C (n=3). **(G)** mRNA expression levels of *RBM3* using mouse primary myoblasts at 32<sup>0</sup>C and 37<sup>0</sup>C at 48 hrs. and 72 hrs. respectively, where the x-axis represents the temperature and the y-axis represents the mRNA fold change of *RBM3* normalized to 18S rRNA and compared to 37<sup>0</sup>C (n=2). **(H)** Western blot analysis of *RBM3* using C2C12 cells at 32<sup>0</sup>C and 37<sup>0</sup>C at 72 hrs. (n=2). **(I)** Western blot analysis of *RBM3* using mouse primary myoblasts at 32<sup>0</sup>C and 37<sup>0</sup>C at 48 hrs. and 72 hrs. respectively (n=2).

**Figure 3**

bioRxiv preprint doi: <https://doi.org/10.1101/2023.05.05.539524>; this version posted May 5, 2023. The copyright holder for this preprint (which was not certified by peer review) is the author/funder, who has granted bioRxiv a license to display the preprint in perpetuity. It is made available under a [CC-BY-NC-ND 4.0 International license](#).

(A)

48 hrs

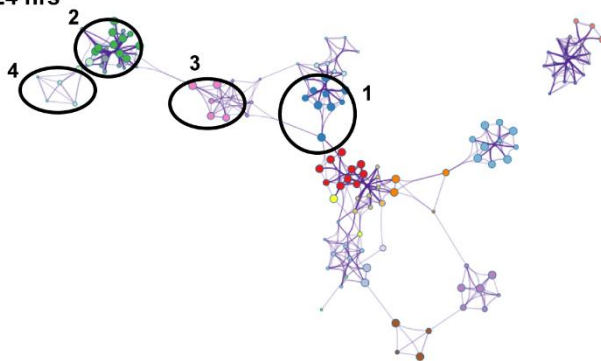


Pathway and process enrichment analysis

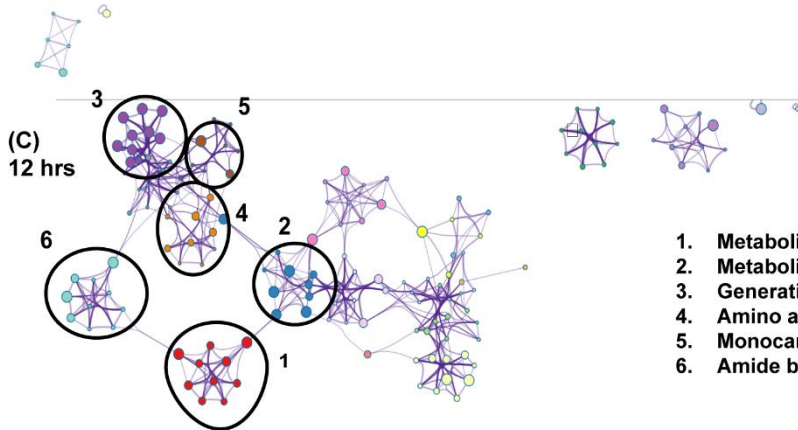
1. Generation of precursor metabolites and energy
2. Monocarboxylic acid metabolic process
3. Metabolism of RNA
4. Amino acid metabolism

(B)

24 hrs



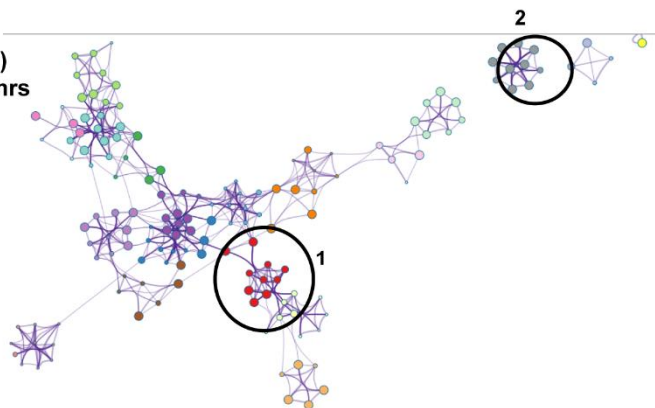
1. Metabolism of RNA
2. Ribose phosphate metabolic process
3. Peptide metabolic process
4. Monocarboxylic acid metabolic process



(C)  
12 hrs

1. Metabolism of RNA
2. Metabolism of amino acids and derivatives
3. Generation of precursor metabolites and energy
4. Amino acid metabolic process
5. Monocarboxylic acid metabolic process
6. Amide biosynthetic process

(D)  
6 hrs



1. Metabolism of RNA
2. Ribonucleotide biosynthetic process

**Figure 3 GO enrichment analysis of protein functional network of C2C12 cells in hypothermia (32<sup>0</sup>C) at 6, 12, 24 and 48 hrs.** GO enrichment protein functional network at (A) 48 hrs. (B) 24 hrs. (C) 12 hrs. (D) 6 hrs. (n=3).

## Figure 4

bioRxiv preprint doi: <https://doi.org/10.1101/2023.05.05.539524>; this version posted May 5, 2023. The copyright holder for this preprint (which was not certified by peer review) is the author/funder, who has granted bioRxiv a license to display the preprint in perpetuity. It is made available under a [CC-BY-NC-ND 4.0 International license](https://creativecommons.org/licenses/by-nc-nd/4.0/).

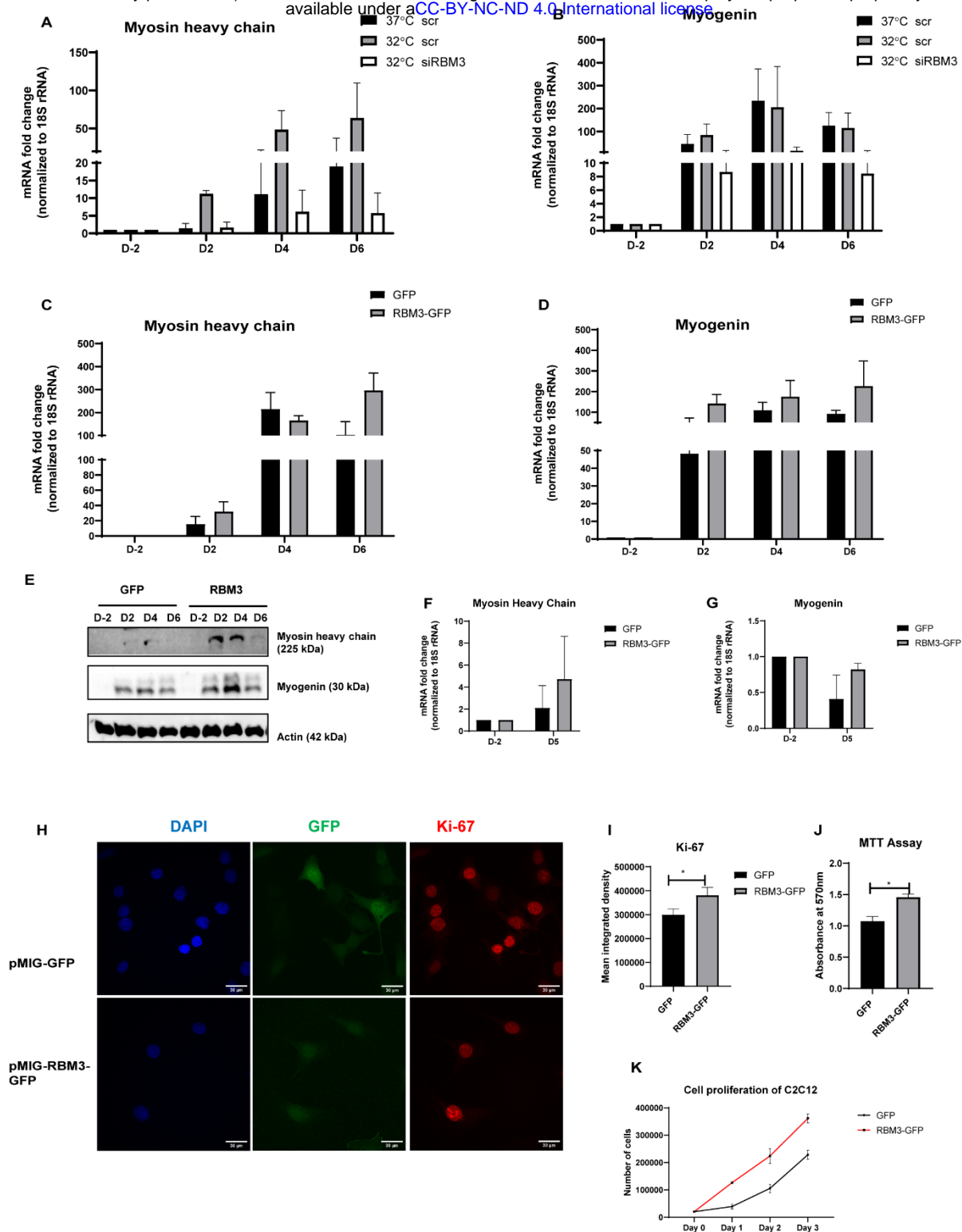


**Figure 4 RBM3 promotes differentiation and viability of skeletal muscle myoblasts. (A)** mRNA expression levels of *MyHC* for siRBM3 and scrambled control (scr) treatment using C2C12 cells at 32°C and 37°C (n=2), where the x-axis represents the number of days pre-differentiation and during differentiation and the y-axis represents the mRNA fold change of

**(A)** mRNA expression levels of *MyHC* normalized to 18S rRNA and compared to D-2. **(B)** mRNA expression levels of *Myog* for siRBM3 and scrambled control (scr) treatment using C2C12 cells at 32<sup>0</sup>C and 37<sup>0</sup>C (n=2), where the x-axis represents the number of days pre-differentiation and during differentiation and the y-axis represents the mRNA fold change of *Myog* normalized to 18S rRNA and compared to D-2. **(C)** mRNA expression levels of *MyHC* during differentiation using C2C12 cells overexpressing pMIG-GFP control and pMIG-RBM3 at 37<sup>0</sup>C (n=3), where the x-axis represents the number of days pre-differentiation and during differentiation and the y-axis represents the mRNA fold change of *MyHC* normalized to 18S rRNA and compared to D-2. **(D)** mRNA expression levels of *Myog* during differentiation using C2C12 cells overexpressing pMIG-GFP control and pMIG-RBM3 at 37<sup>0</sup>C (n=3), where the x-axis represents the number of days pre-differentiation and during differentiation and the y-axis represents the mRNA fold change of *Myog* normalized to 18S rRNA and compared to D-2. **(E)** Western blot analysis of MyHC and MYOG during differentiation using C2C12 cells overexpressing pMIG-GFP control and pMIG-RBM3 at 37<sup>0</sup>C (n=2). **(F)** mRNA expression levels of *MyHC* during differentiation using mouse primary myoblasts overexpressing pMIG-GFP control and pMIG-RBM3 at 37<sup>0</sup>C (n=2), where the x-axis represents the number of days pre-differentiation and during differentiation and the y-axis represents the mRNA fold change of *MyHC* normalized to 18S rRNA and compared to D-2. **(G)** mRNA expression levels of *Myog* during differentiation using mouse primary myoblasts overexpressing pMIG-GFP control and pMIG-RBM3 at 37<sup>0</sup>C (n=2), where the x-axis represents the number of days pre-differentiation and during differentiation and the y-axis represents the mRNA fold change of *Myog* normalized to 18S rRNA and compared to D-2. **(H)** Confocal images of C2C12 cells overexpressing pMIG-GFP control and pMIG-RBM3 at 37<sup>0</sup>C. Red indicates Ki-67 staining, blue indicates DAPI, and Green indicate GFP (Scale bar, 30um). **(I)** Bar graph representing the quantitation of Ki-67 staining where the y-axis represents the mean integrated density of Ki-67 positive nucleus stain. **(J)** Bar graph for MTT assay using C2C12 cells overexpressing pMIG-GFP control and pMIG-RBM3 at 37<sup>0</sup>C where the Y axis represents absorbance at 570 nm (n=3). **(K)** Line graph indicating cell proliferation of C2C12 cells overexpressing pMIG-GFP control and pMIG-RBM3 at 37<sup>0</sup>C where the Y-axis represents the total number of cells and X-axis represents time in days (n=3). \*, \*\*, \*\*\* represents p-value < 0.05, 0.01 and 0.001 respectively.

## Figure 5

bioRxiv preprint doi: <https://doi.org/10.1101/2023.05.05.539524>; this version posted May 5, 2023. The copyright holder for this preprint (which was not certified by peer review) is the author/funder, who has granted bioRxiv a license to display the preprint in perpetuity. It is made available under a [CC-BY-NC-ND 4.0 International license](https://creativecommons.org/licenses/by-nc-nd/4.0/).



**Figure 5 Proteomic mapping of C2C12 cells overexpressing RBM3.** Heat map of upregulated proteins involved in (A) RNA metabolism and processing. (B) lipid metabolism. (C) ETC. (D) Venn diagram representing the upregulated proteins in 48 hrs. hypothermic

(E) GO enrichment pathway analysis of upregulated proteins in RBM3 overexpression (n=3).

Figure 6

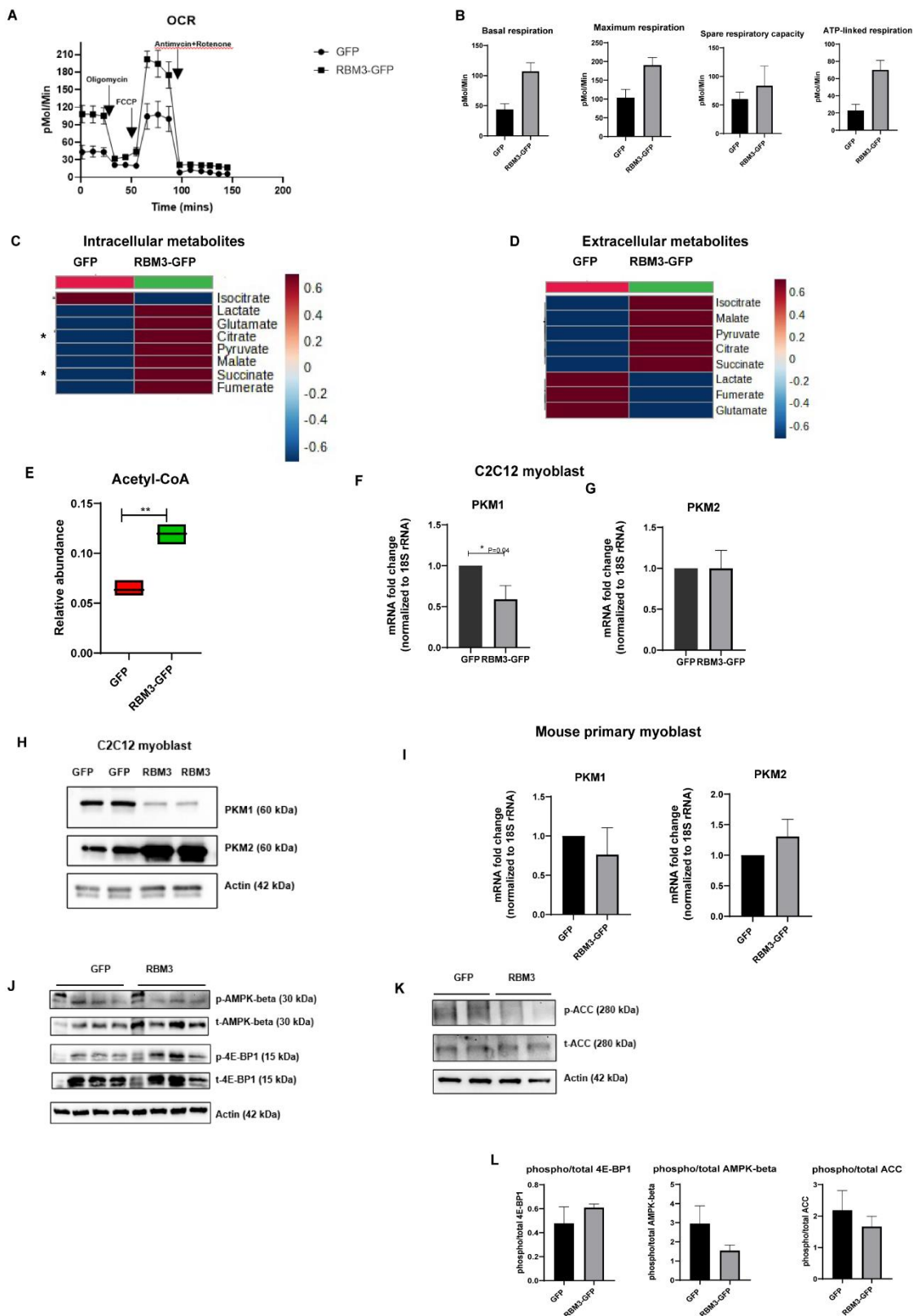


**Figure 6 RBM3 promotes mitochondrial metabolism of skeletal muscle myoblasts. (A)**

Graph showing the mitochondrial OCR of C2C12 cells overexpressing pMIG GFP and pMIG RBM3-GFP, basal OCR and OCR after treatment with oligomycin (1 uM), FCCP (3 uM), antimycin and rotenone (1.5 uM), where the x-axis represents time in minutes and the y-axis represents oxygen consumption rate in pMol/min. **(B)** Bar graph measuring the basal respiration, maximum respiration (OCR after FCCP addition), spare respiratory capacity (basal respiration-maximum respiration) and ATP-linked respiration (basal respiration-respiration after oligomycin addition) of C2C12 cells overexpressing pMIG-GFP and pMIG-RBM3 GFP where the y-axis represents oxygen consumption rate in pMol/Min (n=2). **(C)** Heat map showing levels of TCA metabolites using C2C12 cells overexpressing pMIG-GFP control and pMIG-RBM3. **(D)** Heat map showing levels of TCA metabolites using media (48 hrs.) from C2C12 cells overexpressing pMIG-GFP control and pMIG-RBM3 (n=3). **(E)** Graphical representation of levels of acetyl-CoA using C2C12 cells overexpressing pMIG-GFP control and pMIG-RBM3 (n=3). mRNA expression levels of glycolytic genes **(F)** *PKM1*, **(G)** *PKM2* in C2C12 overexpressing pMIG-GFP control and pMIG-RBM3. **(H)** Western blot analysis of glycolytic protein levels (PKM1, PKM2) using C2C12 cells overexpressing pMIG-GFP control and pMIG-RBM3. **(I)** mRNA expression levels of glycolytic genes *PKM1*, *PKM2* in mouse primary myoblasts overexpressing pMIG-GFP control and pMIG-RBM3 (n=3). **(J)** Western blot analysis of AMPK-beta and 4E-BP1 using C2C12 cells overexpressing pMIG-GFP control and pMIG-RBM3. **(K)** Western blot analysis of acetyl-CoA carboxylase (ACC) using C2C12 cells overexpressing pMIG-GFP control and pMIG-RBM3. **(L)** Bar graph quantifying phosphorylated/total 4E-BP1, ACC and AMPK-beta respectively. \*, \*\*, \*\*\* represents p-value < 0.05, 0.01 and 0.001 respectively.

## Figure 7

bioRxiv preprint doi: <https://doi.org/10.1101/2023.05.05.539524>; this version posted May 5, 2023. The copyright holder for this preprint (which was not certified by peer review) is the author/funder, who has granted bioRxiv a license to display the preprint in perpetuity. It is made available under a [CC-BY-NC-ND 4.0 International license](https://creativecommons.org/licenses/by-nc-nd/4.0/).

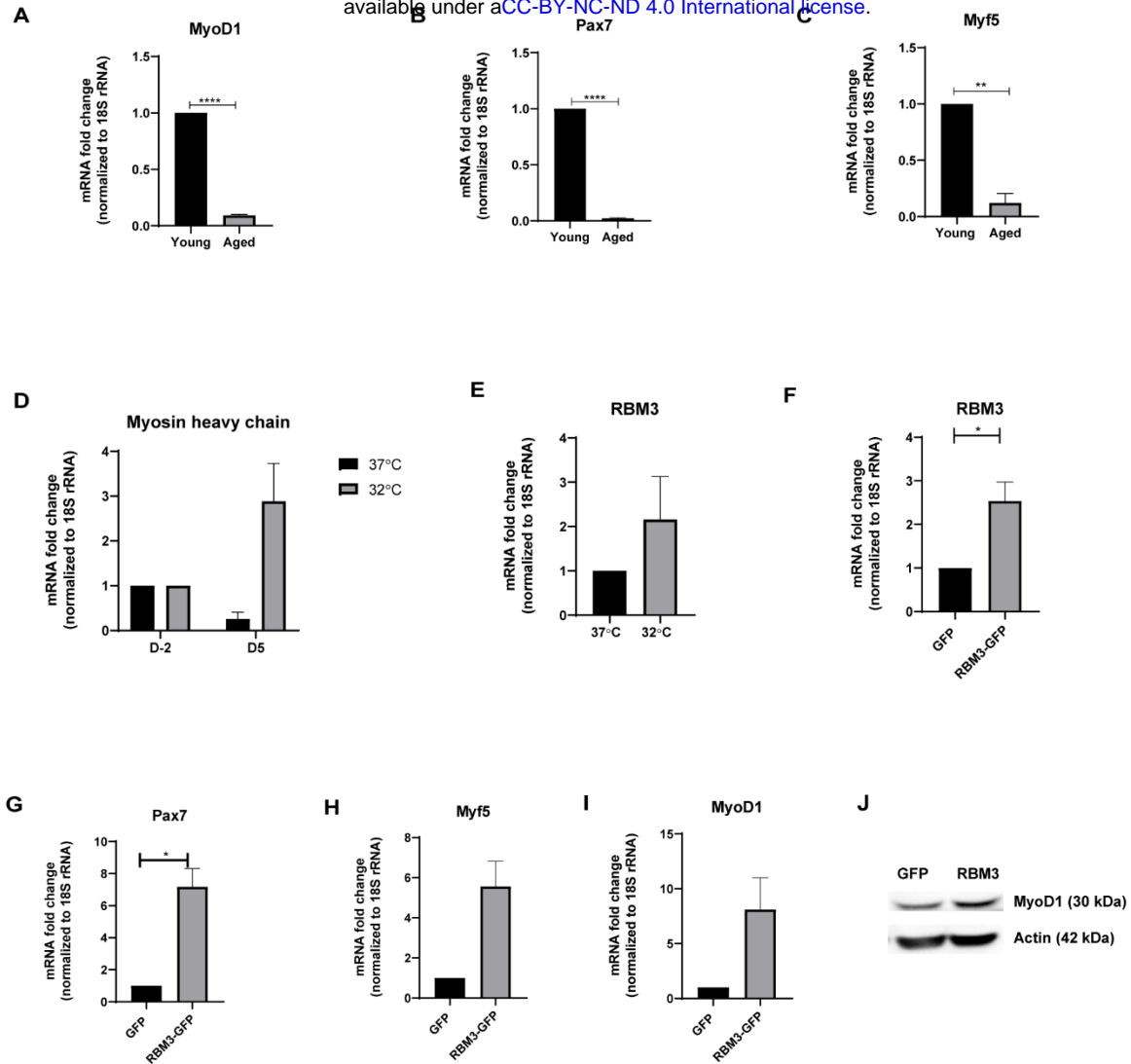


**Figure 7: Overexpression of RBM3 increases stem cell markers in aged myoblasts.** mRNA expression levels of (A) *MyoD1* (B) *Pax7* (C) *Myf5* in aged myoblasts compared to young (D) mRNA expression levels of *MyHC* in aged myoblasts at 32°C compared to 37°C. (n=2) (E) mRNA expression levels of *RBM3* in aged myoblasts at 32°C compared to 37°C. mRNA expression levels of (F) *RBM3*, (G) *Pax7*, (H) *Myf5*, (I) *MyoD1* in aged myoblasts transfected with *RBM3* and control GFP. (n=2 for all the mRNA studies) (J) Western blot analysis of *MyoD1* using mouse primary myoblasts at proliferative stage (72 hrs. post-transfection) overexpressing *RBM3-GFP* and GFP control (n=2). \*, \*\*, \*\*\* represents p-value < 0.05, 0.01 and 0.001 respectively.

**Figure 8**

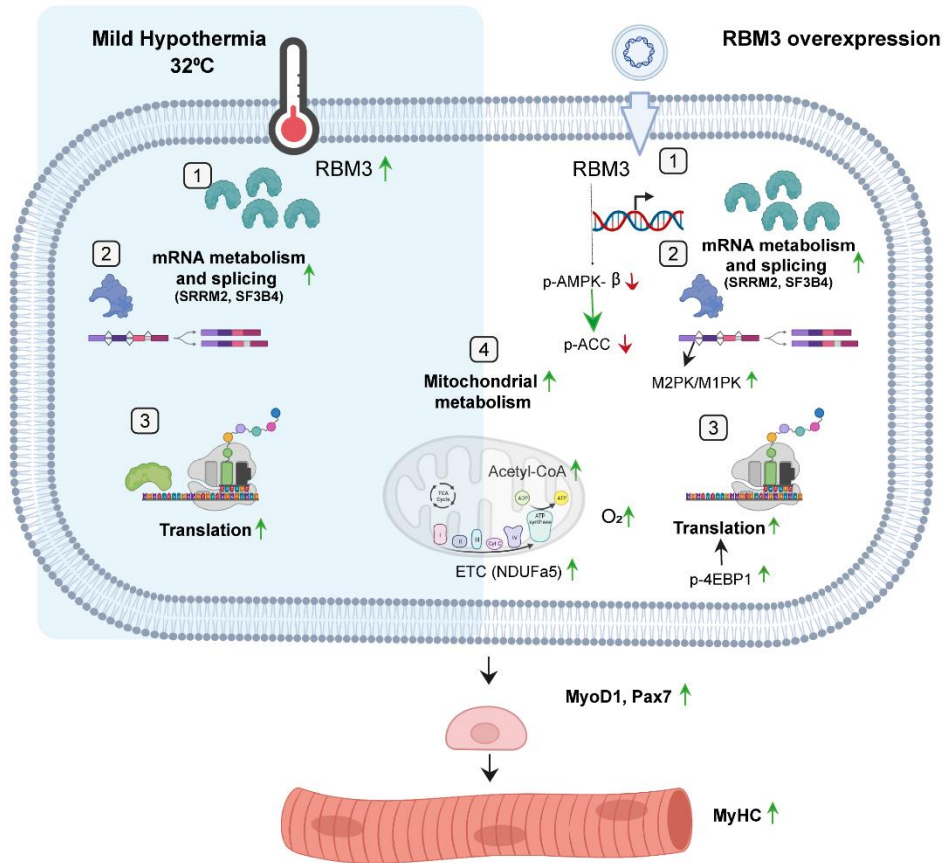


**Figure 8:** Graphical representation showing the effect of mild hypothermia and RBM3 overexpression on important cellular processes like RBM3 expression (1), RNA metabolism and splicing (2), translation (3) and mitochondrial metabolism (4) which finally leads to improved skeletal muscle regeneration.